INVESTIGATION OF WARPING EFFECT ON COUPLED TORSIONAL-AXIAL VIBRATIONS OF DRILLING TOOL

By

NARAHARA GOPAL KOYA

Bachelor of Science in Mechanical Engineering

Acharya Nagarjuna University

Vijayawada, Andhra Pradesh, India.

2013

Submitted to the Faculty of the
Graduate College of the
Oklahoma State University
in partial fulfillment of
the requirements for
the Degree of
MASTER OF SCIENCE
December, 2015

INVESTIGATION OF WARPING EFFECT ON

COUPLED TORSIONAL-AXIAL VIBRATIONS OF

DRILLING TOOL

Thesis Approved:

Dr. Xiaoliang Jin

Thesis Adviser

Dr. Ronald Delahoussaye

Dr. James Manimala

ACKNOWLEDGEMENTS

I would like to express my sincere gratitude to my graduate advisor and mentor, Dr. Xiaoliang Jin for his continuous support and motivation during my master's study and research. He enlightened me with the first glance of research. It was him who welcomed me into his research group and provided some valuable ideas to choose my research topic. The knowledge he shared with me, the kind of trust he had in me, the kind of patience he showed when correcting my mistakes, are some things that made me admire him a lot. I am extremely fortunate to have an advisor like him. Without Dr. Jin, this research work would not have been completed or written.

Besides my advisor, I would like to thank Dr. Ronald Delahoussaye and Dr. James Manimala for being on my committee. I would also like to thank Dr. Prabhakar Pagilla for letting me use the Laser Doppler vibrometer equipment in his lab.

I would also like to extend my sincere thanks to the school of mechanical and aerospace engineering at Oklahoma State University for giving me the opportunity to pursue my graduate education.

I thank my colleagues at Precision Manufacturing Processes Lab: Anju, Arjun and Boyuan for the stimulating discussions, for the sleepless nights working on research, and for all the fun that we had in the past two years. I greatly value their friendship and moral support at my difficult times. I also thank my friends Surya, Suresh, Nakul and Theja for coping up with me from the past 2 years during my stay in Stillwater.

My friends supported me to stay same during these difficult years. The care and support they showed, helped me overcome the hitches in my life and stay focused on my research. Their friendship is invaluable and I am extremely grateful for having such an awesome friends. I cannot list all the names here, but I take this opportunity to thank each and every friend of mine for being with me.

Finally, I would like to acknowledge, with deepest gratitude, the support and immeasurable love of my family. My elder brother, Siva Koya has been my best companion throughout my life. He deserves my whole hearted thanks for the kind of support and guidance he provided me since our childhood. My parents, Jhansi and Sambasiva Rao have supported me at each and every phase of my career. They gave me freedom to take my own decisions and gave up many things for me to chase my dreams. I can never be grateful enough to such an amazing parents. Nothing is happier to me than making them feel proud for my achievements.

Name: NARAHARA GOPAL KOYA

Date of Degree: DECEMBER, 2015

Title of Study: INVESTIGATION OF WARPING EFFECT ON COUPLED TORSIONAL-AXIAL VIBRATIONS OF DRILLING TOOL

Major Field: MECHANICAL AND AEROSPACE ENGINEERING

Abstract:

Coupled torsional-axial vibration of the drilling tool plays a significant role in the machining dynamics of the drilling process. The torsional-axial vibration of the drilling tool due to the warping deformation of the pretwisted flute is modeled in this thesis. The warping dependent cross sectional properties of the drill flute are obtained from proposed 2D finite element method. Natural frequency and mode shape corresponding to the torsional-axial vibration of the drill are predicted with experimental validation. The effects of helix angle, web thickness and aspect ratio on the coupled torsional-axial dynamics are analyzed for conventional and micro drills. The proposed model is able to provide optimum geometric configuration of the drilling tool for required torsional-axial dynamic behavior with high computational efficiency, and guide the drilling process in order to reach desired hole quality.

Clamping boundary conditions highly influences the drilling tool dynamics. An enhanced receptance coupling model is developed to predict coupled torsional-axial vibrations of the drilling tool considering the dynamics of fixing structure and clamping conditions. Rigid and flexible receptance coupling methods are used to predict the dynamics of the drilling tool including the joint dynamics between the tool and the tool-holder. Experimental validation of the predicted results indicates the efficiency of the proposed model in obtaining the exact dynamics of the drilling tool considering the clamping boundary conditions.

Keywords: Drilling tool, Warping deformation, Coupled torsional-axial dynamics, 2D finite element method, receptance coupling.

TABLE OF CONTENTS

Chapter Page

LIST OF TABLES

LIST OF FIGURES

Figure Page

Figure Page

CHAPTER I

INTRODUCTION

1.1 Coupled Torsional-Axial Dynamics of Drilling Process

Drilling operation is widely used to generate machined holes on a workpiece using conventional and micro drilling tools. Typically, drills with diameters less than 2 mm are classified as micro drills. The schematic of conventional and micro drilling process is shown in Figure 1.1, with different types of machined holes shown in Figure 1.2. Drilling process has most common applications in aerospace and automotive industries. Dynamics of drilling tool plays a significant role in cutting force, chatter stability and hole quality in the drilling process. The types of drilling tool vibrations include lateral, axial-torsional and whirling movements [1, 2]. Due to the complex fluted cross section of drilling tool, dynamics of drilling process are not studied to the same extent as milling or turning. In milling and turning operations, the tool vibration is predominantly in bending direction. Whereas in drilling, the tool shortens or elongates as its twists or untwists, leading to a complex coupled torsional-axial vibration behavior. This coupled vibration depends on the geometric parameters of the drilling tool such as drill diameter, helix angle, aspect ratio and web thickness, and the clamping boundary conditions. The coupled torsional-axial vibration of drilling tool has to be modeled accurately in order to improve the productivity and hole quality.

Figure 1.1 Drilling process. (a) Conventional drilling (b) Micro-drilling [3, 4].

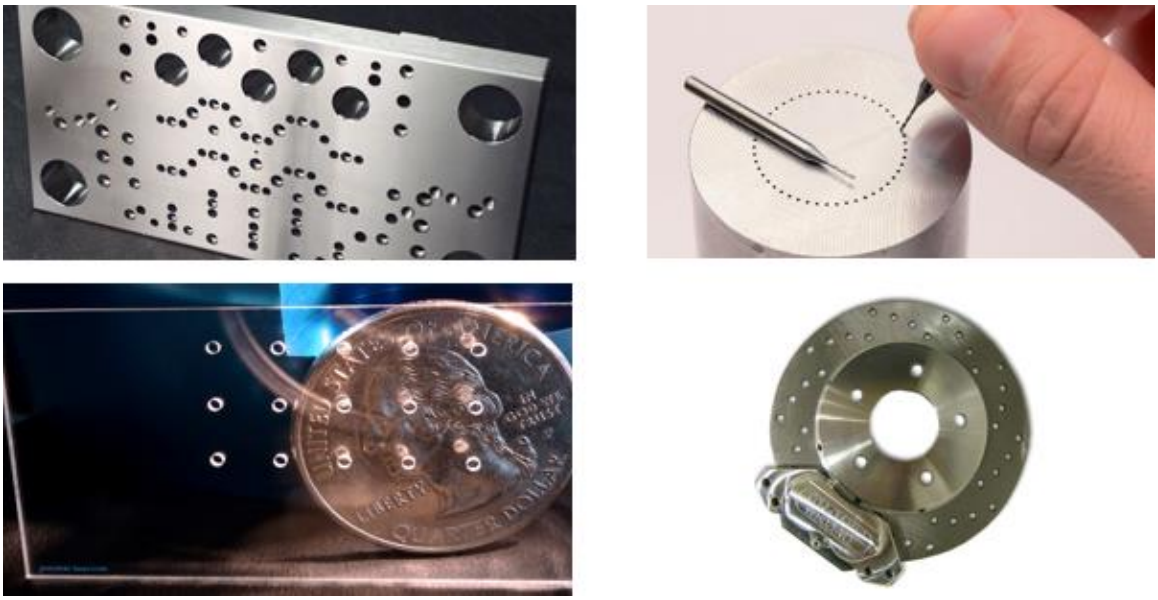

Figure 1.2 Different types of micro and macro machined holes [5, 6, 7, 8].

The coupling of torsional and axial vibrations in the dynamics of a drilling tool are mainly due to the pre-twisted flute geometry. Typically, the flute section of a drilling tool is modeled as a non-circular pre-twisted beam that exhibits coupling between torsional and axial vibrations [9]. It is known that torsional rigidity of a beam increases when a pretwist is induced into the geometry.

This was first explained by Wagner's hypothesis [10] in which the beam is assumed to be made of straight fibers when it is in untwisted state. When the beam is twisted, these fibers are not straight anymore but are twisted along the length of the beam. Hence, if there is any axial force on the beam, it would produce a couple resulting from the twisted fibers. This theory has been the base for many researchers over the decades in understanding the coupled torsional-axial vibration behavior. Later, because of the inaccuracies in Wagner's hypothesis which assumes coupling phenomenon in a cylindrical beam, Saint-Venant torsion theory was used to model that the coupling effect in pretwisted beams is due to the effect of initial twist on the warping related cross section properties of the beam. Warping of a cross section is defined as axial deformation along the beam axis when torque is applied about the same axis. Accurate prediction of the cross section properties of any non-circular beam is needed in order to analyze the effect of pretwist. There are several cross section properties of interest which are important to understand the dynamics of the drilling tool, including warping-dependent and warping-independent cross section properties. Warping independent cross section properties include area of cross section, moments of inertia etc, while warping dependent cross section properties include torsion constant and other constants that are related to the pretwist which are discussed in chapter 3. However, closed-form analytical solutions exist only for a few common non-circular cross section shapes such as elliptical or triangular shapes. There are no analytical solutions for complex cross section geometries in the case of drilling tool. On the other hand, Finite Element (FE) Method can be used by dividing the domain of cross section into a number of small elements, and numerically evaluating the cross section properties for each element and finally providing the pretwist properties for whole drilling tool. As element-based functions are used to approximate the cross section properties, the computational efficiency of the model increases significantly without losing predictive accuracy.

Natural frequencies and mode shapes are the dominant dynamic parameters in evaluating structure vibrations. In the drilling process, the dynamic property of drilling tool has to be

understood in order to select proper conditions to avoid excessive forced vibrations or self-excited vibrations of the tool. Natural frequencies and mode shapes corresponding to coupled torsional-axial vibration must be determined beforehand so that unnecessary vibration of the tool can be avoided and process production can be increased. The coupled vibration is related to a variety of geometric parameters of the drilling tool such as helix angle, aspect ratio, and web thickness etc. In order to select the optimum geometric configuration of the drilling tool for required torsional-axial dynamic behavior, it is important to investigate the effect of various geometric parameters on the coupled torsional-axial vibration phenomenon. Determining the relationship between torsional-axial dynamics and geometry of the drilling tool using commercial finite element (FE) software requires extensive computational effort, since any geometric change requires remodeling of the tool structure. Hence, there is a need to develop a model which is able to predict the dynamics of the drilling tool with high computational efficiency and predictive accuracy.

In the actual machining process, the self-excited regenerative chatter vibration limits the applications of drilling tools in high-speed machining. The overall productivity of the system and hole quality are greatly reduced due to chatter vibrations. Conventionally, dynamics of the drilling tool are predicted using a cantilever approximation for the tool with one end completely fixed in the tool holder. However, the dynamics of drilling tool are highly influenced by the dynamics of spindle and the joint between the tool and the holder, shown in Figure 1.3. Hence, prediction of the tool dynamics considering clamping dynamics is needed to suppress the chatter vibrations. Such a prediction of actual dynamics can be performed by using receptance coupling method [11]. A receptance coupling technique enhanced for the prediction of coupled torsional-axial receptances is proposed in this thesis and used for the prediction of drilling tool dynamics. The details of this method are discussed in the chapter 4.

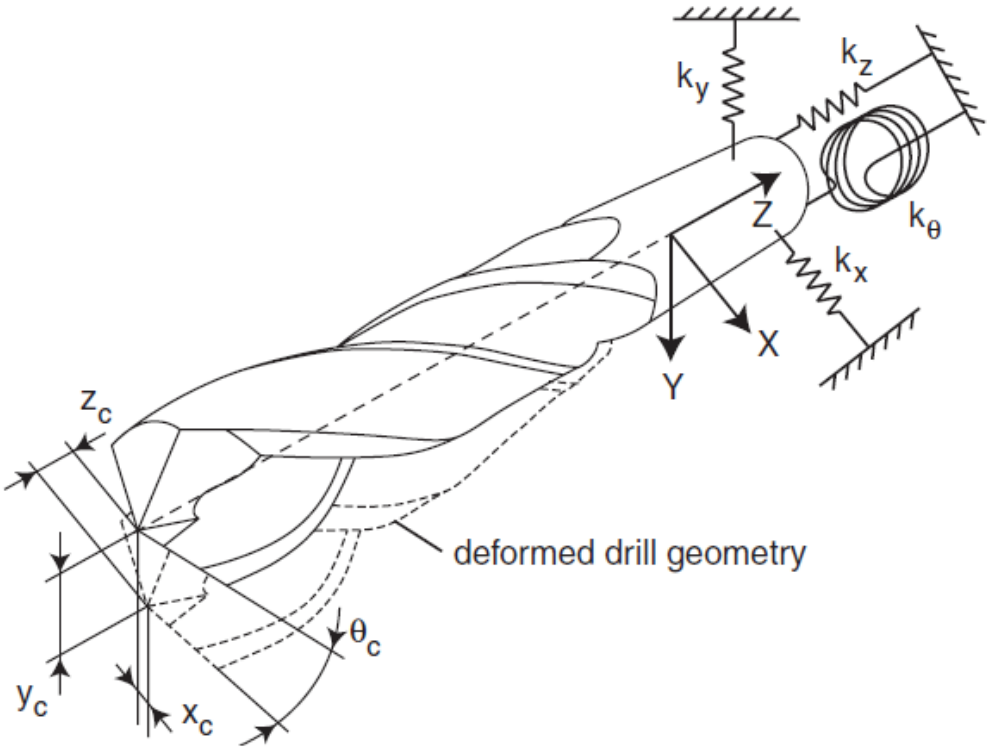

Figure 1.3 Dynamic model of a drilling tool showing deflections in Axial, Torsional and bending directions [1].

1.2 Objectives and Approach

This thesis addresses the importance of coupled torsional-axial vibrations of the drilling tool for evaluating the overall drilling performance. The objective of this study is to predict the coupled torsional-axial vibration behavior of drilling tool which is critical to process efficiency and hole quality in drilling process including the warping deformation. This research enables the modeling of drilling tool dynamics with high computational efficiency and predictive accuracy. The effects of geometric parameters such as helix angle, web thickness and aspect ratio on the tool dynamics are analyzed. The effect of boundary condition on the drilling tool dynamics is predicted using enhanced receptance coupling technique. The outcome of this research provides an efficient way to select optimum geometric configuration of the drilling tool for required dynamic behavior and also predicts the dynamics of the drilling process with the effect of boundary condition. The

outcome of this thesis is able to facilitate proper selection of cutting conditions to reduce unnecessary vibrations and improve hole quality in both conventional and micro drilling processes.

In this thesis, warping properties of the cross section which influences the coupled torsional-axial dynamics are determined. The natural frequencies and mode shapes of the drilling tool in free-free boundary conditions are predicted. 2D FE method is used since no analytical solution is available to obtain the warping and stress functions for the complex cross section of the drill. The prediction accuracy of the model is validated by experiments using a Laser Doppler Vibrometer (LDV). The effects of geometric parameters of the drilling tool on the coupled torsional-axial dynamics are analyzed. Receptance coupling technique is used to model the effect of clamping boundary conditions on the coupled torsional-axial dynamics of the drilling tool. The results are verified through experiments.

CHAPTER II

LITERATURE REVIEW

2.1 Pretwisted Beam Dynamics

In this thesis, the drilling tool is modeled as a pretwisted beam that exhibits coupled vibration between torsional and axial directions [9]. Over the past years, research on the dynamics of pretwisted beams has been conducted to investigate the coupling phenomenon between axial and torsional vibrations, with the applications in dynamic analysis of aircraft blades, turbine blades and helicopter blades. This phenomenon was initially approached through an assumption that the pretwisted beam consists of helical fibers running along the length of the beam. Modeling of coupling phenomenon was first put forward by Wagner [10] and it was found that the torsional rigidity of the beam increases with the pretwist. Biot and Goodier [12] also predicted that the torsional stiffness of a prismatic beam increases subjected to axial loading. It was stated that the effect of increasing torsional stiffness is significant only for sections with low torsional rigidity. Chu [13] applied the theory to thin prismatic bars and tubular members and was able to match the results with previous theories. All the above theories are later concluded to be flawed as they predicted the increase in torsional stiffness for a circular beam subjected to pretwist. They used the theory of elasticity which is applicable only for orthogonal coordinate system in the case where non-orthogonal system of coordinates were supposed to be used. Hence these theories were limited to thin-walled cross section with small pretwist.

Later, it was found by Rosen [14] that the increase in torsional rigidity of pretwisted beams is due to the effect of pretwist on the warping function of the beam. It was proposed that there is no warping for beams with circular cross section, thereby solving the helical fiber assumption and hence pretwist does not have any effect on circular cross section beams. Saint-Venant torsion theory was used to derive the warping related constants that are critical in understanding the warping effects on pretwist. Quantitative relationship between the increase in torsional rigidity and initial twist was established and it was proved that circular cross section was not affected by pretwist. This theory was later extended to simultaneous actions of non-linear torsion and extension [15]. Hodges [16] used a similar approach to Rosen and concentrated on torsion of pretwisted beams under axial loading. A new approach instead of Saint-Venant torsion theory [17] was proposed to characterize the beam's warping function using the components of Green strain tensor. The coupling phenomenon between axial-torsional vibrations was demonstrated. Shield [18] studied the same coupling as Hodges and extended the theory to beams whose axis of pretwist is off centered from the centroidal axis. Krenk [19] proposed a linear theory for pretwisted elastic beams subjected to homogenous loading and accounted for shear center, the elastic center and the pretwist axis. Later, an asymptotic solution was proposed by expansion of the three dimensional terms of linear elasticity [20], and Kosmatka [21] studied the coupling vibrations of the beams with torsion and axial deformation coupled with bending.

Rosen [22] provided a review of all the research that has been concentrated on the dynamics of pretwisted beams and emphasized the importance of pretwisted beams in many engineering applications along with the complexity of modelling them. Recently, Liu et al [23] studied the torsional-axial coupling of pretwisted beams and addressed the importance of neglecting the higher order terms in the derivation of warping function using Saint-Venant Torsion theory. Through scaling analysis, they were able to provide a validation criteria under which the common

assumptions are normally valid. This thesis analyzes the dynamics of the drilling tool with the flute section based on the equations of motion proposed by Rosen [15] for pretwisted beam.

2.2 Solution for warping function

The mechanics of pretwisted beams suggests that the initial twist of the beam influences the warping properties of the cross section. However, validations in most of the research works are performed using pretwisted beams with elliptical or triangular cross sections for which analytical solutions exist to find warping function. If the dynamics of a pretwisted beam with an irregular cross section are to be known, the cross section properties related to warping deformation should be calculated beforehand. Theocaris [24] provided the solution based on Saint-Venant torsion theory for the warping function using caustics of the warped cross section. Caustics are the reflection of light rays from an arbitrary cross section that characterize the shape of cross section. Warping function solution was obtained based on the properties of caustic obtained from the cross section geometry. But evaluating the equations of caustics for irregular cross sections is a time-consuming and practically impossible in certain circumstances. Hence, numerical approximations, such as finite element method can be used for solving the torsion problem and determining various cross section properties [25].

The most common formulation of the torsion problem is given in terms of Prandtl stress function [26]. A finite element tool to solve the problem of torsion subjected to Neumann and Dirichlet boundary conditions is provided by Jochen Alberty et al [27]. The domain of the boundary was divided into a number of triangular and quadrilateral elements and then incorporated the Neumann and Dirichlet boundary conditions to solve the reduced linear system. Mixon [28] applied this solution to solve the warping function and determined the warping related cross section properties of the cross section. This thesis solves the warping function using Dirichlet boundary

conditions and additional warping related cross section properties specific to the cross section geometry of drilling tool.

2.3 Coupled Torsional-Axial Dynamics of the drilling tool

Coupled Torsional-Axial vibrations play a significant role in the drilling stability and hole quality of the drilling process. Based on the results from D.H Hodges [16], Bayly et al. [9] proposed a chatter vibration model of the twist drills including the torsional-axial coupled vibration. Chatter stability lobes for drilling were predicted. The coupled torsional-axial phenomenon creates a wavy surface finish on the bottom of the drilled hole. The results were able to confirm that torsional-axial coupling was responsible for the low quality of hole in the drilling process. Roukema and Altintas [29] provided a two dimensional time domain simulation model for torsional-axial chatter. Drilling tool was modeled as a pretwisted beam. Experimental cutting forces and the sound of drilling process were studied in order to analyze the vibration behavior of the drilling tool. The mechanistic cutting force model proposed was able to predict the cutting forces and surface finish. This model was later extended to lateral vibrations of the drilling tool. The coupling between lateral and coupled torsional-axial vibrations in the machining process were discussed. Chatter stability of the drilling process corresponding to lateral and torsional-axial vibrations were predicted and experimentally verified using cutting tests [30]. A similar cutting force model was presented by Imani and Moosavi [31]. Dynamic undeformed chip thickness was studied based on boundary conditions of the drilling tool. Boundary conditions were modeled to be clamped-free at the beginning of drilling process and clamped-pin when the drilling tool is engaged into the work piece. Cutting force simulation results for different boundary conditions were verified by experimental results. A four degree of freedom model for drilling tool vibrations was provided by Ahmadi and Altintas [32]. Effect of process damping is considered in the model. Chatter stability diagrams corresponding to lateral, torsional-axial vibrations were predicted and experimentally verified. Influence of torsional-axial vibration on the chip formation of the tool was studied by Voronov et

al [33]. The character of torsional-axial chatter in the unstable region of the drilling process was studied. The cutting forces, displacements and chip shapes in the drilling process were predicted. Overall, these research demonstrated the importance of coupled torsional-axial vibration of tool on the drilling dynamics and hole quality.

Filiz and Ozdoganlar [34] proposed a two dimensional model to characterize the coupled torsional-axial vibrations of micro and macro drills. Using polynomial mapping, the drill cross section was mapped to a rectangular domain and spectral-Tchebychev polynomial technique [35] was used to model the cross section parameters of the drilling tool. The accuracy of the model depends on the size of cross section as it was observed that the accuracy in the case of micro drills is higher than macro drills. The same technique was also used for end mills [36, 37]. A three dimensional approach was proposed later using spectral-Tchebychev technique to develop a model for the dynamics of micro and macro drills [38, 39, 40]. However, it was found that the accuracy of the model depends on the size of cross section. As the size of cross section increases, more polynomials are needed to accurately predict the dynamics which increases the time consumption and decreases computational efficiency. Moreover, only first coupled torsional-axial natural frequency is considered.

Based on the related research in the literature, it is demonstrated that the coupled torsional-axial vibration behavior of drilling tool plays a significant role in the drilling process. Also, it is observed that there is a requirement for a model which can predict the dynamics of drilling tool with high computational efficiency and predictive accuracy. In this thesis work, a new model for coupled torsional-axial dynamics of the drilling tool is developed considering the warping deformation of the cross section and pretwist rate of the drilling tool. Natural frequencies and Mode shapes corresponding to the coupled torsional-axial vibration are predicted with high computational efficiency and experimentally validated, and the effects of geometric parameters on the drilling tool dynamics are predicted.

2.4 Receptance Coupling for the prediction of tool dynamics

In the actual drilling process, the dynamics of the drilling tool are influenced by the supporting structure (which includes tool holder, spindle head and other parts of the machine). Imani and Moosavi [31] conducted the drilling experiments but they considered clamped-free boundary condition for the drilling tool when fixed in the tool holder. Tool holder, in general cannot clamp the drilling tool with perfectly infinite stiffness and hence it changes the dynamics of the drilling process. Generally, spindle head and tool holder are the most flexible parts of the machine structure and their dynamics influences the dynamics of drilling tool. In order to understand the complete dynamics of the drilling process, dynamics of the tool holder and other parts of the machine have to be modeled. Analytical modeling of the parts of complete machine structure is practically impossible as the damping and stiffness parameters at each joint of the machine are unknown. Hence, experimental techniques need to be implemented to effectively capture the dynamics of machine structure. While experimental techniques can predict the FRF directly at the tool tip, it is time consuming in some applications where the tool is to be changed more frequently. Hence, a predictive technique based on structural engineering was proposed by Schmitz et al [41, 42] which eliminated the time consuming repetitive FRF measurement. It was shown that there is a dramatic variation in the tool point response as the tool modes interact with the tool holder/spindle modes. Simon Park et al [43] used the receptance coupling technique to predict the dynamics of end mills. The receptance coupling technique was improved by considering the dynamics in both translational and rotational degrees of freedom. A short blank cylinder with the same material as the tool was used to measure the dynamics of spindle assembly. The rotational dynamics are extracted mathematically from the direct and cross FRF measurements. This ensured the coupling of various end mills of different sizes to the spindle without making repetitive FRF measurements. The model was able to identify chatter free cutting conditions in milling process. The same technique was also applied to micro milling tools [44]. Schmitz and Duncan [45] provided a multi-

point receptance coupling approach that can couple nested components with same neutral axis. A three-component receptance coupling technique was proposed for the prediction of tool point dynamics by dividing machine tool-holder-spindle into three substructures [46]. The above research works used rigid coupling to join the substructures into an assembly. In a machining process, where a number of tools have to be changed frequently, rigid receptance coupling technique cannot be used because the existence of joint between the tool and the tool holder is flexible. Hence, the existence of joint dynamics need to be predicted using flexible receptance coupling technique in order to capture the exact dynamics. Park and Chae [47, 48] proposed a receptance coupling considering the joint dynamics of modular tools. Modular tools may not be present in all machining processes and in most of the machining processes the whole tool have to be changed. Hence, joint dynamics need to be identified near the tool-holder. All the above mentioned research are concentrated on lateral vibrations and rotations of the spindle-tool assembly.

Schmitz [49] extended the receptance coupling technique to be used for the prediction of torsional and axial receptances. The torsional and axial FRF at tool points are predicted with experimental validations. However, the receptances corresponding to the coupled torsional-axial vibration was not considered in the model. In this thesis work, two enhanced receptance coupling models including both rigid coupling and flexible coupling for the prediction of the coupled torsional-axial vibration of the drilling tool are proposed, and applied to predict the tool point FRF of the drilling tool with experimental validation.

CHAPTER III

MODELLING OF COUPLED TORSIONAL-AXIAL VIBRATIONS OF DRILLING TOOL

3.1 Determination of Warping Constants of Cross Section

The cross section of a pretwisted beam continuously rotates with respect to the longitudinal axis. When a torque is applied in the direction of pretwist, it creates stresses in the longitudinal direction and causes elongation or contraction of the beam, depending on the direction of the torque. Similarly, the pretwisted beam has rotational motion when an axial force is applied. The varying stress in the cross section causes warping deformation of the beam. The flute section of the drilling tool can be modeled as a pretwisted beam with a non-circular cross section which shows coupling between torsional and axial vibrations. Based on the principle of virtual work, the deformation of pretwisted beam under simultaneously acting axial force and torsional moment are expressed as [15]:

$$EA\epsilon + ES\theta + \frac{1}{2}EI_p\theta^2 = T \tag{3.1}$$

$$ES\epsilon + (GJ_s + EK)\,\theta + EI_p\epsilon\,\theta + \tfrac{3}{2}ED\theta^2 + \tfrac{1}{2}EF\theta^3 = M \tag{3.2}$$

where the axial and torsional strains ϵ and θ are coupled with the axial force T and moment M. The linear terms (*EK*, *ES*) and the non-linear terms ($\frac{1}{2}EI_p\theta^2$, $EI_p\epsilon\,\theta$, $\frac{3}{2}ED\theta^2$, $\frac{1}{2}EF\theta^3$) represent the change in torsional and axial rigidity due to initial twist. *K*, *S*, *D*, *F* are the section integrals which depend on the warping function ω of the cross section, expressed as:

$$J_s = \iint_A \left[\left(-z + \frac{\partial\omega(x,y,z)}{\partial y}\right)^2 + \left(y + \frac{\partial\omega(x,y,z)}{\partial y}\right)^2\right] dy\,dz \tag{3.3a}$$

$$I_p = \iint_A (y^2 + z^2)\; dy\,dz \tag{3.3b}$$

$$K = \iint_A \left(\frac{\partial\omega(x,y,z)}{\partial x}\right)^2 dy\,dz \tag{3.3c}$$

$$S = \iint_A \left(\frac{\partial\omega(x,y,z)}{\partial x}\right) dy\,dz \tag{3.3d}$$

$$D = \iint_A \left(\frac{\partial\omega(x,y,z)}{\partial x}\right)(y^2 + z^2)\; dy\,dz \tag{3.3e}$$

$$F = \iint_A (y^2 + z^2)^2\, dy\,dz \tag{3.3f}$$

Determination of the integrals in Equations (3.3) requires obtaining the warping function with respect to the geometry of the tool's cross section. The contour of the cross section depends on the helix angle h_0, point angle ρ and web thickness W. The exact contour geometry of the drilling tool is characterized by the following equation [50, 51, 52]:

$$\psi = \sin^{-1}\frac{W}{2r} + \frac{\sqrt{r^2 - \left(\frac{W}{2}\right)^2}}{R}\tan h_o \cot\rho \tag{3.4}$$

where (r, ψ) are in polar coordinates.

Figure 3.1 shows the nomenclature of the of the drilling tool and Figure 3.2 shows the cross sections of the drill with the same diameter and different helix angles. It is evident that cross sectional properties are highly sensitive to the helix angle of the drilling tool.

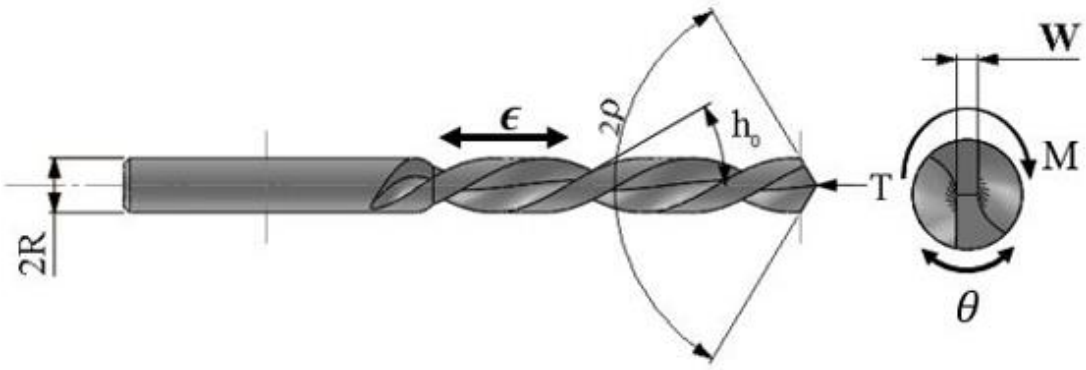

Figure 3.1 Drilling tool Nomenclature.

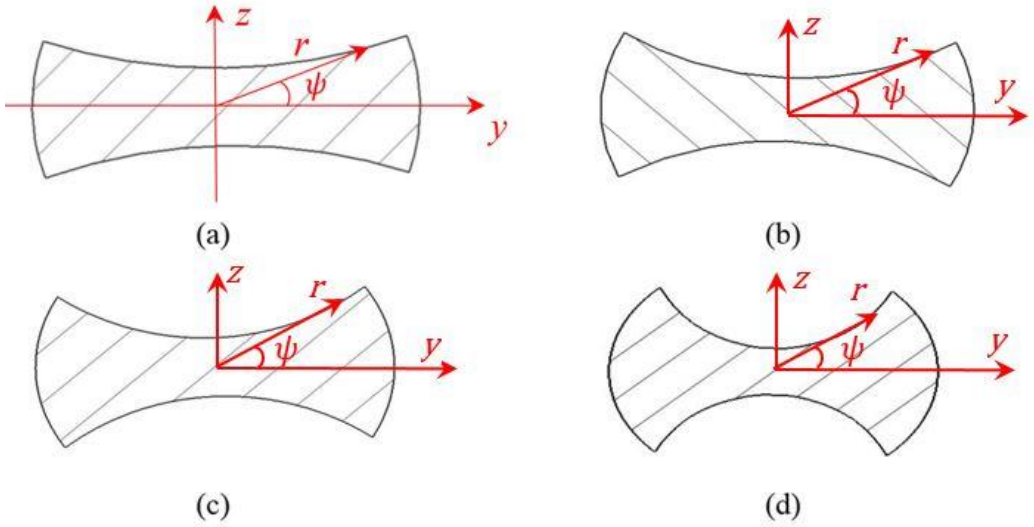

Figure 3.2 Cross sections of a drill with different helix angles. (a) 15˚, (b) 25˚, (c) 30˚, (d) 45˚.

Based on Saint-Venant torsion theory [26, 53], the warping function is related to the Prandtl stress function, $\Phi(y, z)$, given as:

$$\tau_{xy} = G\theta \left[\frac{\partial \omega(x,y,z)}{\partial y} - z\right] = \frac{\partial \Phi(y,z)}{\partial z} \qquad (3.5a)$$

$$\tau_{xz} = G\theta\left[\frac{\partial\omega(x,y,z)}{\partial z} + y\right] = -\frac{\partial\Phi(\mathrm{y,z})}{\partial \mathrm{y}} \tag{3.5b}$$

where θ is the angle of twist per unit length and, ω is the warping function expressed in the orthogonal coordinates (x, y, z), shown in Figure 3.1.

Therefore, the warping function can be obtained from the stress function based on Equation (3.5):

$$\frac{\partial\omega(x,y,z)}{\partial y} = \frac{1}{G\theta}\frac{\partial\Phi(\mathrm{y,z})}{\partial z} + z \tag{3.6a}$$

$$\frac{\partial\omega(x,y,z)}{\partial z} = -\frac{1}{G\theta}\frac{\partial\Phi(\mathrm{y,z})}{\partial \mathrm{y}} - y \tag{3.6b}$$

The stress function is constant along the boundary of the cross section, and it is expressed as:

$$\nabla^2\Phi(\mathrm{y,z}) = -2G\theta \quad \text{with} \quad \nabla^2 = \frac{\partial^2}{\partial y^2} + \frac{\partial^2}{\partial z^2} \tag{3.7}$$

The formulations provided in Equations (3.5), (3.6) and (3.7) are partial differential equations for which analytical solutions doesn't exist for the cross section shapes shown in Figure 3.1. Hence, FE method which was originally used to characterize general area cross section properties (torsion constant, area moments of inertia) [28] of pretwisted beam is applied in this study to derive the warping related properties (*K, S, D* in Equation (3.3)) for the cross section of drilling tool. The cross section of the drilling tool is meshed using three node triangular elements [54]. The cross section of the drill is modelled using 751 nodes and 1400 three node triangular elements in order to maintain the prediction accuracy. One quadrant of the cross section is meshed and the property of symmetry is applied to obtain the final results, shown as Figure 3.3.

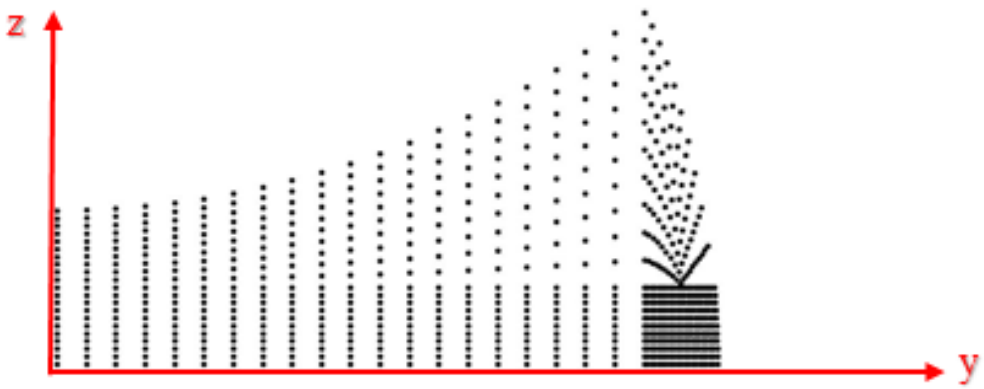

Figure 3.3 Mesh of the drilling tool cross section.

Linear shape functions are used to define the displacements of the elements, and defined as:

$$N_i = \frac{1}{2A_e}[a_i + b_i y + c_i z] \tag{3.8}$$

where $a_i = y_j z_k - y_k z_j \quad b_i = z_j - z_k \quad c_i = -(y_j - y_k)$ and i, j, k represent the node number for each element and are equal to 1, 2, 3 consecutively.

The y, z coordinates of the cross section are interpolated for elements using the shape functions as follows:

$$y_e = [N_1 \quad N_2 \quad N_3]\begin{bmatrix} y_1 \\ y_2 \\ y_3 \end{bmatrix} and\ z_e = [N_1 \quad N_2 \quad N_3]\begin{bmatrix} z_1 \\ z_2 \\ z_3 \end{bmatrix} \tag{3.9}$$

Integrals of shape functions are evaluated as:

$$\int_{A_e} {N_1}^a {N_2}^b {N_3}^c \, dA_e = 2A_e \frac{a!\, b!\, c!}{(a+b+c+2)!} \tag{3.10}$$

where cross sectional area of the element is given as

$$A_e = \frac{1}{2}\det\begin{vmatrix} 1 & y_1 & z_1 \\ 1 & y_2 & z_2 \\ 1 & y_3 & z_3 \end{vmatrix} \tag{3.11}$$

Therefore, the warping related constants for the cross section of the drilling tool given in Equation (3.3) are obtained as follows:

$$J_s = 2\int_{A_e} \Phi \, dA = \frac{2A_e}{3}[\Phi_1 + \Phi_2 + \Phi_3] \tag{3.12a}$$

$$K = k^2 \iint_A \left(y^2 + z^2 + y\frac{\partial \Phi}{\partial \mathrm{y}} + z\frac{\partial \Phi}{\partial z}\right)^2 dy\, dz \tag{3.12b}$$

$$S = k \iint_A \left(y^2 + z^2 + y\frac{\partial \Phi}{\partial \mathrm{y}} + z\frac{\partial \Phi}{\partial z}\right) dy\, dz \tag{3.12c}$$

$$D = k \iint_A \left(y^2 + z^2 + y\frac{\partial \Phi}{\partial \mathrm{y}} + z\frac{\partial \Phi}{\partial z}\right)(y^2 + z^2)\, dy\, dz \tag{3.12d}$$

By substituting $\Phi = [N_1 \quad N_2 \quad N_3]\begin{bmatrix}\Phi_1 \\ \Phi_2 \\ \Phi_3\end{bmatrix}$ into Equations (3.12), the warping related cross section constants are evaluated from shape functions, with the derivations described in Appendix 1.

3.2 Prediction of Coupled Torsional-Axial Dynamics of Drilling Tool

After the warping related constants are evaluated, Equations (3.1) and (3.2) which describe the mechanics of pretwisted beam can be used to model the stiffness matrix of the coupled torsional-axial dynamics of the drilling tool. It is found that the equations are nonlinear due to the involvement of higher order terms of angular strain θ. Sensitive studies are performed on a conventional drill with 10mm diameter and a micro drill with 0.5 mm diameter to investigate the values of nonlinear terms compared to the corresponding linear terms. Typical ranges of force and torque are applied and the values of non-linear terms are obtained. For conventional drill, 1300 N axial force and 11 Nm torque are applied, and for micro drill, 12 N axial force and 0.004 Nm torque are used. From Table 3.1, it is observed that the values of all the non-linear terms are less than 1% compared to their corresponding linear terms.

Table 3.1 Comparison of non-linear terms with corresponding linear terms in Equations (3.1) and (3.2).

Non-linear terms	Corresponding linear terms	Ratio between non-linear and linear terms	
		Conventional Drill (10 mm Diameter)	Micro Drill (0.5 mm Diameter)
$\frac{1}{2}EI_p\theta$	ES	0.5786%	0.9164%
$EI_p\epsilon$	$(GJ_s + EK)$	-0.4570%	-0.5595%
$\frac{3}{2}ED\theta$	$(GJ_s + EK)$	0.1619%	0.2178%
$\frac{1}{2}EF\theta^2$	$(GJ_s + EK)$	0.0047%	0.0099%

Therefore, it is concluded that the non-linear terms in Equations (3.1) and (3.2) can be neglected for the dynamic analysis in typical drilling operations, and the linear relation between axial force, torque and axial, torsional strain for each element in axial direction are given:

$$T = C_{11}\epsilon + C_{12}\theta \tag{3.13}$$

$$M = C_{21}\epsilon + C_{22}\theta \tag{3.14}$$

where $C_{11} = \frac{EA}{L}, C_{12} = C_{21} = \frac{ES}{L}, C_{22} = \frac{GJ_s+EK}{L}$. The warping constant S represents the coupled torsional-axial dynamics, and K represents the increase of the torsional rigidity due to pretwist. The drilling tool is separated into shank and flute sections, and each section is divided by 100 elements along the axial direction. L is the length of each element of the drill.

The linearized model of the torsional-axial mechanics of the drill can be used to formulate the stiffness matrix in the dynamic model shown in Equation (3.15). For each element, the characteristic equation is expressed as:

$$([K] - \omega_n^2[M])[U] = 0 \tag{3.15}$$

where the stiffness matrix is: [K] = $\begin{bmatrix} C_{11} & C_{12} & -C_{11} & -C_{12} \\ C_{21} & C_{22} & -C_{21} & -C_{22} \\ -C_{11} & -C_{12} & C_{11} & C_{12} \\ -C_{21} & -C_{22} & C_{21} & C_{22} \end{bmatrix}$, mass matrix is $[M] = \begin{bmatrix} \frac{mL}{3} & 0 & \frac{mL}{6} & 0 \\ 0 & \frac{IL}{3} & 0 & \frac{IL}{6} \\ \frac{mL}{6} & 0 & \frac{mL}{3} & 0 \\ 0 & \frac{IL}{6} & 0 & \frac{IL}{3} \end{bmatrix}$, ω_n is the natural frequency, and the mode shape for torsional-axial displacement is $[U] = [U_1 \quad \Theta_1 \quad U_2 \quad \Theta_2]^T$.

The elemental matrices are then combined to form global matrices along the axial direction of the drilling tool, and the eigenvalue/eigenvector problem is solved to obtain the natural frequencies and the mode shapes.

3.3 Experimental Validation

3.3.1 Experimental Setup and Measurement Procedure

Modal testing is conducted to experimentally obtain the natural frequencies and the mode shapes of the drilling tool to validate the model. A miniature force hammer is used to apply impact on the drilling tool in axial direction. A Polytec™ Laser Doppler Vibrometer is used to measure the axial and torsional displacements of the drilling tool. The measurement setup is shown in Figure 3.4. The drill is hanged by two elastic bands to secure the drill in position against the laser sensor. Elastic bands are used in such a way that their presence will not affect the torsional-axial vibration modes, shown in Figure 3.4 (b). Therefore, free-free boundary condition corresponding to torsional-axial dynamics can be approximated. A National Instruments™ data acquisition card is used to capture the excitation and response signals. Commercial software CutPro™ [55] is used to control the modal testing procedure and obtain the frequency response function (FRF). In order to obtain the mode shape of the drilling tool, the axial and rotational displacements need to be measured at different locations along the axial direction of tool. Therefore, small plates with

dimensions of 4x3 mm^2 are attached to the drilling tool with approximately 10 mm distance interval. The impulse hammer is excited at the tip of the drilling tool in axial direction, and the responses of the plates at different locations of the tool are measured by LDV. The FRFs corresponding to the torsional-axial vibrations are obtained, from which the natural frequencies and mode shapes are identified in both axial and torsional directions.

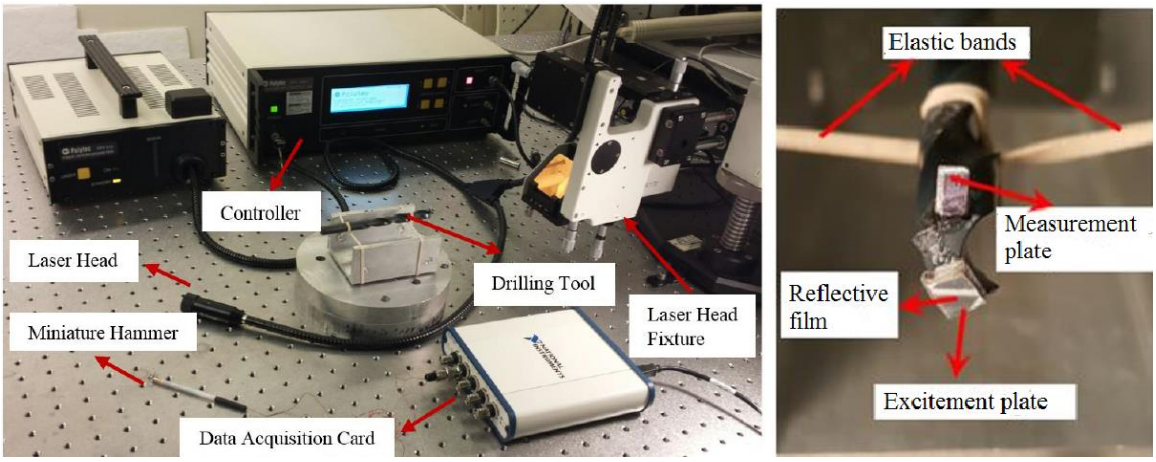

(a) (b)

Figure 3.4 Experimental setup for modal testing on drilling tool (a) LDV and hammer test equipment along with drilling tool fixed in free-free boundary condition (b) Small plates attached to the drilling tool to facilitate LDV measurements and excitation.

Two conventional drilling tools with different geometries are used for experimental validation. The diameter, lengths of shank and flute section of the tool are labeled in Figure 3.4, and the corresponding values are shown in Table 3.2. The material of the drilling tool is high speed steel, with elastic modulus E=235 GPa, Poisson's ratio υ = 0.28, and density ρ = 7700 kg/m^3. Web thickness of the drilling tool is 20% of the total drill diameter.

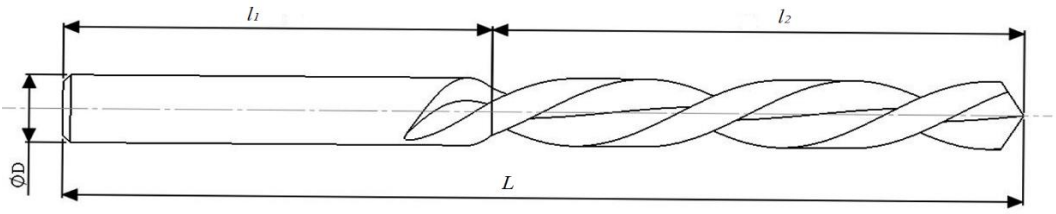

Figure 3.4 Geometry of the conventional drilling tool.

Table 3.2 Specifications of conventional drilling tools (All dimensions are in mm unless specified).

Drill	l_1	l_2	L	D	Helix angle (°)
D1	67.0	66.0	133.0	10.0	30.0
D2	64.0	29.0	93.0	4.88	15.0

3.3.2 Results and Analysis

The dynamic properties of the drilling tool highly depend on the warping related cross sectional constants given in Equations (3.13) and (3.14). Based on the geometric specifications of the two drilling tools given in Table 3.2, the proposed 2D FE method is used to obtain the flute section cross sectional constants, and the calculated values are shown in Table 3.3. Thereafter, the global stiffness and mass matrices corresponding to the coupled torsional-axial vibrations of the tool are obtained, and the natural frequencies are calculated by solving the eigenvalues of the characteristic Equation (3.15). The first three natural frequencies corresponding to the torsional-axial modes obtained from the proposed model are compared with the results from commercial FE software and the experiments, shown in Table 3.4. Using parametric spline equation, the shape of the cross section is modeled and is twisted along the helix with given drill parameters to form the flute portion of the drilling tool. Then, the shank portion is attached as a solid body to the flute portion of the drilling tool. It is found that the proposed 2D FE model predicts the natural frequencies corresponding to coupled torsional-axial vibration mode of the drilling tool with less

than 6% error compared to the commercial FE and experimental results. The deviation may be due to the discretization of the drilling tool in the FE model, and the elastic band in the experimental setup may cause minor modification of the tool's boundary condition in axial or torsional direction. Commercial FE simulations were conducted on a computer with 6 Gb RAM and 3.4 GHz processor. It is proved that the proposed model takes less than 10 seconds to obtain the simulation results, while the computational time using commercial FE software is around 10-15 minutes in average. Thus, the computational efficiency is improved to a large extent based on the proposed model. This is especially beneficial when determining the effect of drilling tool geometry on the coupled torsional-axial dynamics, for which the models with varying geometric features need to be developed and simulated, which will be explained in Section 3.4.

The effect of the attached small plates on the dynamics of the drilling tool is studied. The attached plate is modeled in Solidworks [56], and it is found that the first bending natural frequency of the plate is higher than 40 KHz, which is beyond the first three natural frequencies of the drilling tool. Furthermore, the variation of the natural frequency of the drilling tool due to added mass of the plate is less than 0.5%. Therefore, attaching the small plate on the drill tool is only to facilitate the measurement using LDV, and the influence on the measurement results is negligible.

Table 3.3 Cross sectional properties of drill flute from proposed model.

Drill	A **(m^2)**	S **(m^3)**	K **(m^4)**	I_p **(m^4)**	J_s **(m^4)**
D1	3.067e-05	3.1852e-08	4.7328e-11	3.3621e-10	6.0370e-11
D2	5.933e-06	2.8355e-09	2.1236e-12	1.4041e-11	2.1807e-12

Table 3.4 Comparison of natural frequencies for first three coupled torsional-axial modes for conventional drilling tools.

Natural Frequency (kHz)

Drill	Proposed Model	FE software	Error %	Experiment	Error %
D1	7.2102	7.2435	0.46	7.2603	0.69
	19.0118	18.688	-1.7326	18.0909	-5.09
	20.9945	21.03168	0.1768	21.07797	0.396
D2	8.2584	8.2458	-0.1526	8.2418	-0.20106
	21.2537	21.4935	1.116	22.06539	3.67857
	26.4579	26.526	0.2568	26.56285	0.395106

The mode shapes obtained from the proposed model and experimental measurements for the two conventional drilling tools are shown in Figures 3.5 and 3.6. The solid lines in the graph represent the results predicted by the model, and the diamonds indicate the experimental measurements. All the graphs have length of the drill (in mm) on horizontal axis. For each mode, both the axial and torsional mode shapes are plotted together due to the coupling effect. The comparison shows that the proposed model is able to accurately predict the coupled torsional-axial dynamics modes of the drilling tool with high computational efficiency.

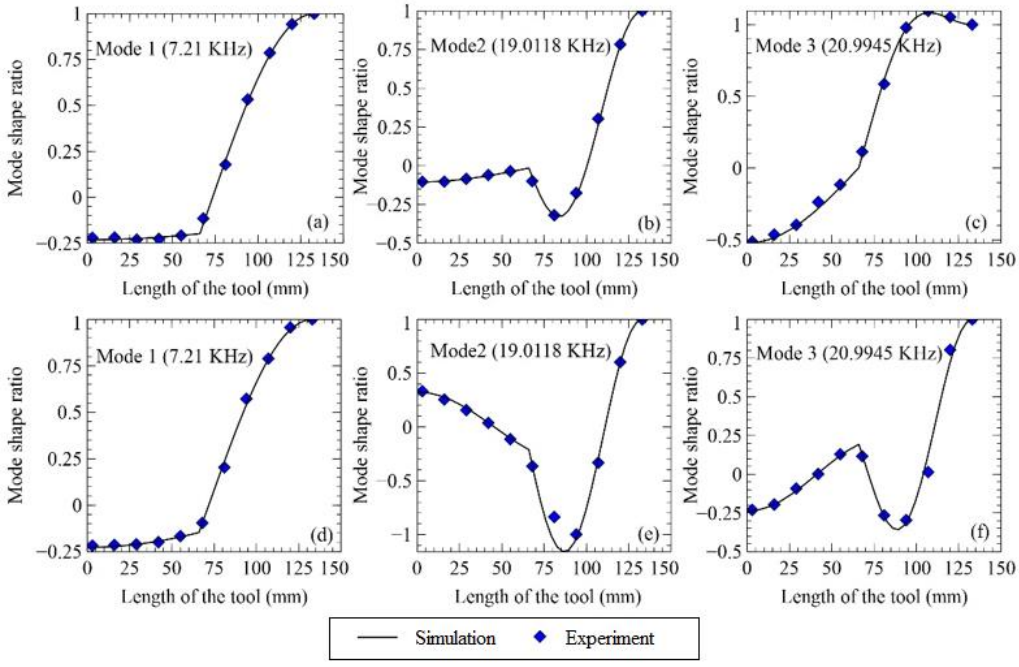

Figure 3.5 Comparison of mode shapes between proposed model and experiments (D1). Length of drilling tool on horizontal axis and displacement ratio on vertical axis. (a), (b), (c) represent the first three axial modes, and (d), (e), (f) represent the first three torsional modes.

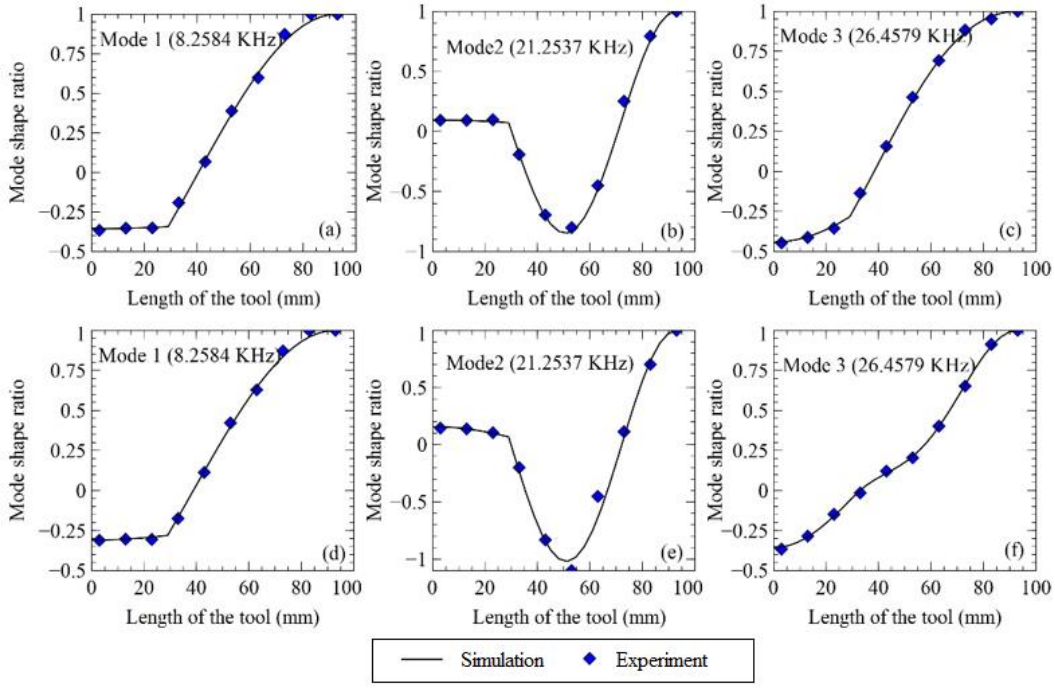

Figure 3.6 Comparison of mode shapes between proposed model and experiments (D2). Length of drilling tool on horizontal axis and displacement ratio on vertical axis. (a), (b), (c) represent the first three axial modes, and (d), (e), (f) represent the first three torsional modes.

3.4 Analyses on the Effect of Tool Geometry on Torsional-Axial Dynamics

Helix angle, web thickness of the cross section, and aspect ratio are the critical geometric features that influence the torsional-axial dynamics of the drilling tool. In this study, the effects of each geometric parameter on the natural frequency of the coupled dynamics are analyzed using proposed model.

3.4.1 Effect of Helix angle

Helix angle is an important parameter that influences the cutting edge strength and the hole accuracy in the drilling process. Typically, the helix angle of drilling tool varies from 10° to 35°. The selection of helix angle depends on the workpiece material, required mechanics and dynamics. Low helix drills provide excellent chip discharge and high tool rigidity which are generally used for applications having high spindle speeds [57], while high helix drills facilitates deep hole drilling and are commonly used at low spindle speeds.

The geometry of the drilling tool in this analysis is based on D1 drill, with all the parameters the same except that the helix angle varies from 5° to 35°. Figures 3.7 (a), (b), (c) show the variations of first three natural frequencies corresponding to torsional-axial dynamics with respect to the helix angle. This is because the warping related cross section constants *S* and *K* increase with the twist rate *k* in equation (12) when helix angle increases, and then the stiffness values C_{12}, C_{21}, C_{22} corresponding to the coupled torsional-axial dynamics in equations (13) and (14) increase. It is observed that all three natural frequencies increase with the helix angle. The first natural frequency increases by 32% and the second natural frequency increases by 25%, while the third frequency increases only by 3% as the helix angle increases from 5^0 to 35^0. This is because the first two modes are torsional vibration dominant, and the torsional stiffness (C_{22} in Equation (3.14)) increases when the warping constant *K* increases. On the other hand, the third natural frequency is axial vibration dominant, and the axial stiffness (C_{11} in Equation (3.13)) is not influenced by the warping constants. The minor change of the third natural frequency is due to the variation of the coupled elements (C_{12} and C_{21}) in the stiffness matrix in Equations (3.13) and (3.14).

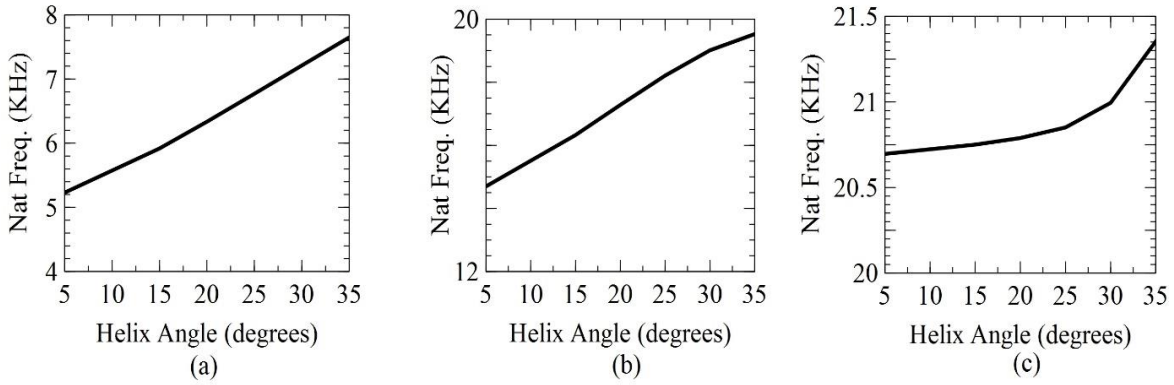

Figure 3.7 Variations of natural frequencies of drilling tool with helix angle. (a), (b) and (c) represent the first three natural frequencies respectively.

3.4.2 Effect of Web thickness

The web thickness of the drill influences the drill rigidity and chip removal ability. Web thickness variations influence the point strength of the drilling tool. Larger web thickness means the drill point needs more thrust to penetrate into the work piece. However, smaller web thickness reduces the chip evacuation ability of the drill. In this study, the effect of web thickness varying from 10 to 20 percent of the drill diameter on the dynamics is investigated. As seen in Figures 3.8 (a), (b), (c), the first natural frequency increases by 23% and second natural frequency increases by 18% as the web thickness goes from 10% to 20% of the total diameter, whereas the third natural frequency changes by less than 0.5%. This is because the increment in web thickness increases the drill stability in torsional direction more than in axial direction. The first two modes of the drill are torsional vibration dominant and the third mode is axial vibration dominant. Hence, the change in the third natural frequency is not obvious compared to the first two as the web thickness varies. The change of web thickness does not change the relative magnitude of elements in the eigenvectors, therefore, the mode shape is not seen to change.

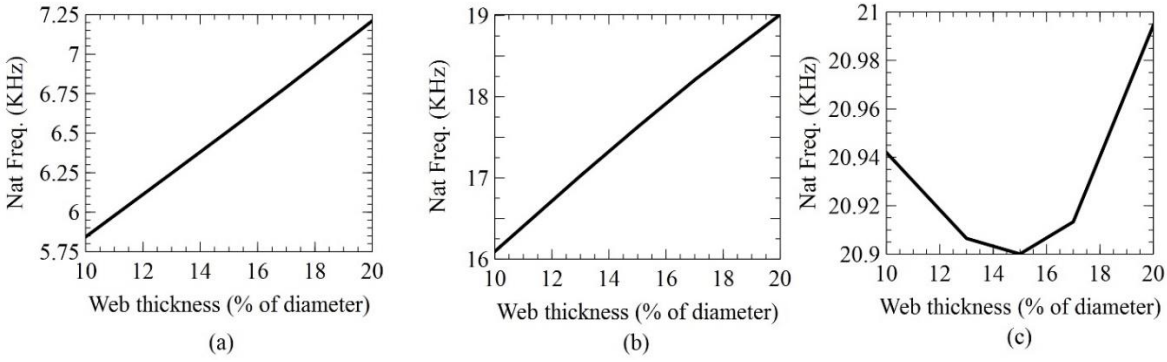

Figure 3.8 Variations of natural frequencies of drilling tool with web thickness. (a), (b) and (c) represent the first three natural frequencies respectively.

3.4.3 Effect of Aspect Ratio (AR)

Aspect ratio is the ratio of the length of the flute to diameter of the drilling tool. High aspect ratio of the drill enables deep hole drilling. However, the rigidity of the tool reduces with the increase of aspect ratio of the drilling tool. Increase of aspect ratio also causes potential bulging of the drilling tool therefore affecting the hole accuracy. Hence, an optimum value of aspect ratio needs to be used based on the analysis of the drilling tool dynamics. As seen in Figures 3.9 (a), (b), (c), when the aspect ratio increases from 4 to 10, the first natural frequency decreases by 55%, second natural frequency decreases by 46% and third natural frequency decreases by 48%. As length of the drill increases, the torsional and axial stiffness of the drill decreases, hence the natural frequencies decrease as well. The change of aspect ratio does not change the relative magnitude of elements in the eigenvectors, so the mode shape does not change.

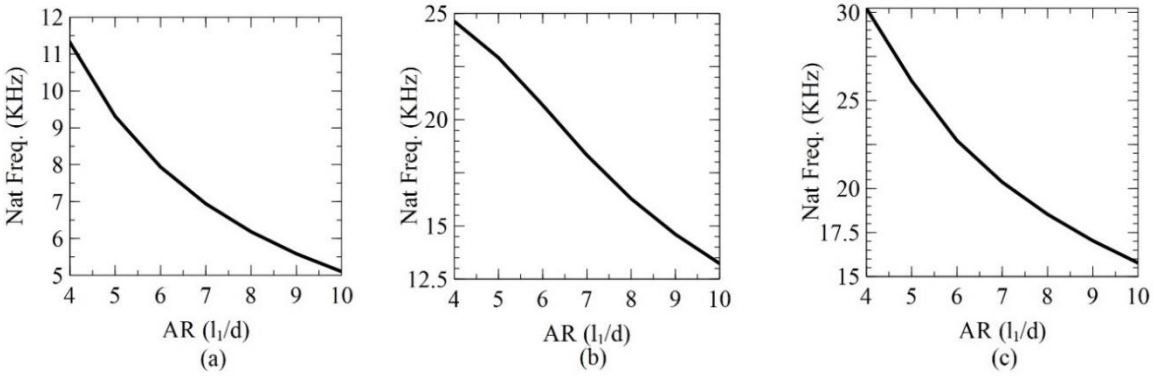

Figure 3.9 Variations in natural frequencies of a conventional drilling tool with change in aspect ratio. (a), (b) and (c) represent the first three natural frequencies respectively.

3.5 Application of the Model to Micro Drill Dynamics

3.5.1 Prediction of Coupled Torsional-Axial Dynamics of Micro Drill

Compared to conventional drilling process, micro drilling is applied to generate miniature holes with accurate geometry and high aspect ratio on a variety of materials. Different from conventional drill in which the diameter of the flute and shank sections are close to each other, the geometry of the micro drill is composed of shank, taper and cutting flute, shown in Figure 3.10. The coupled torsional-axial dynamics of the tool comes from the flute section of the micro drill, and influences the vibrations of shank and taper portions due to rigid mechanical coupling between the three sections. In this study, each section is divided into 50 elements along the axial direction. The proposed 2D FE method is applied to analyze the dynamics of the micro drill with three different geometries, shown in Table 3.5. Commonly used micro drill material tungsten carbide is used in the model, with the elastic modulus E=653 GPa, rigidity modulus G=270 GPa, and density ρ = 15565 kg/m^3. Web thickness of the drilling tool is 20% of the total drill diameter. The warping related cross section parameters calculated by the proposed model are shown in Table 3.6.

Table 3.5 Specifications of micro drills in the simulation (All dimensions in mm unless specified).

Micro Drill	d	l_2	l_3	l_1	D	Helix angle (°)
MD1	1.6	11.2	13.4	38.0	2.0	25.0
MD2	1.0	6.5	8.0	25.0	1.5	30.0
MD3	0.5	3.2	4.0	25.0	1.0	25.0

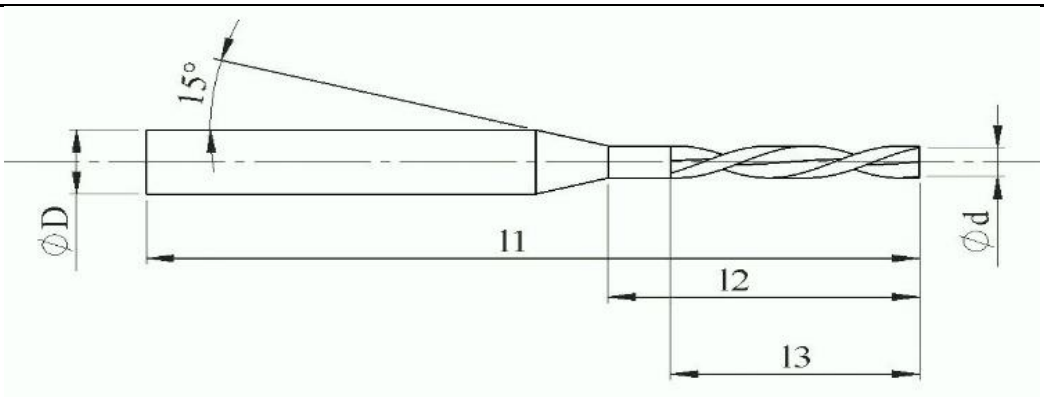

Figure 3.10 Geometry of the micro drill.

Table 3.6 Cross sectional parameters of micro drills.

Micro Drill	A (m^2)	S (m^3)	K (m^4)	I_p (m^4)	J_s (m^4)
MD1	7.33E-07	9.64E-11	1.87E-14	2.00E-13	3.42E-14
MD2	3.07E-07	3.19E-11	4.73E-15	3.36E-14	6.04E-15
MD3	7.16E-08	2.94E-12	1.78E-16	1.90E-15	3.26E-16

The first three natural frequencies corresponding to the coupled torsional-axial modes obtained from 2D FE model are compared with the results from FE software for free-free boundary conditions. The results are listed in Table 3.7. It is found that the proposed model predicts the natural frequencies corresponding to the torsional-axial vibration with less than 2% error compared to the results obtained from commercial FE. Same as conventional drill, computational burden is extensively reduced by the proposed model. Therefore, it is possible to analyze the effect of

geometric feature on the micro drill dynamics with high efficiency. It is found that most of the natural frequencies are larger than 35 kHz. Since the highest frequency bandwidth from the miniature hammer is less than 20 kHz, the experimental modal testing on micro hammer is not performed in this study.

Table 3.7 Comparison of first three torsional-axial coupled natural frequencies for micro drills.

	Natural Frequency (kHz)		
Drill	**Proposed Model**	**FE Software**	**% error**
MD1	35.4186	35.255	0.46404
	47.89092	47.624	0.560479
	56.72406	56.624	0.176705
MD2	57.48319	57.599	-0.20106
	79.40101	79.11	0.367857
	88.51435	88.166	0.395106
MD3	49.31782	49.653	-0.67504
	75.31677	76.726	-1.8367
	145.0629	146.29	-0.83879

3.5.2 Effect of Geometric Parameters on the Dynamics of Micro Drill

The effects of geometric parameters including helix angle, web thickness of the cross section, and aspect ratio on the torsional-axial dynamics of micro drill are described below:

3.5.2.1 Effect of Helix angle

The geometry of MD1 micro drill is selected in this study, with all the parameters being the same except that helix angle varies from 5^0 to 35^0. The first three natural frequencies are shown as Figures 3.11 (a), (b), (c) respectively, with the solid line representing the results from the

proposed model, and the dashed line representing the results from FE software. The proposed model shows that as the helix angle of the flute portion increases, the first natural frequency increases by 36%, while the changes of the second and third natural frequencies are less than 0.5%. The difference of the results between the proposed model and FE software for the first two modes are less than 5%. However, the third natural frequency from FE software decreases by almost 7% as the helix angle increases to 35°. It is observed that the error increases as the helix angles increases. These increasing deviations at higher helix angles are due to the common assumptions from Saint-Venant theory that the warping function for a pretwisted beam is identical to that of a prismatic beam for the same cross section shape [23]. However, the natural frequencies predicted by the model are within 3% error range for commonly used helix angles (25° to 30°).

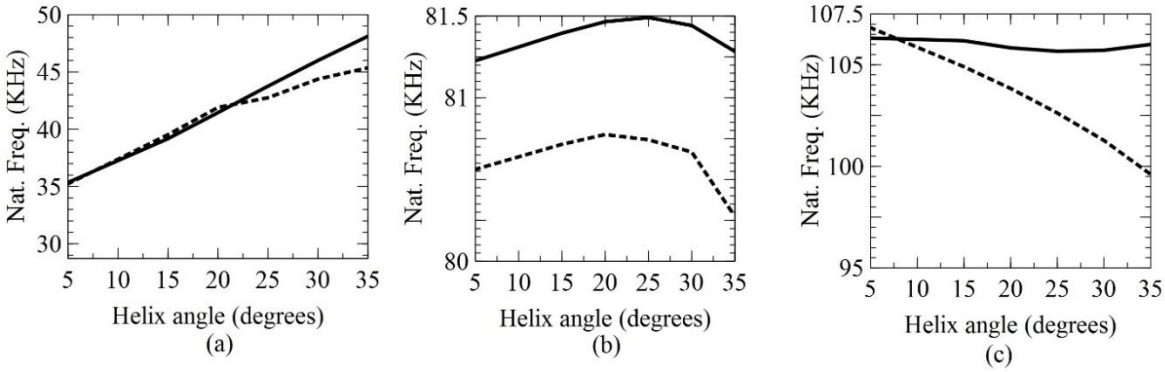

Figure 3.11 Variations of natural frequencies of the micro drill with helix angles. Solid lines represent the variations of natural frequencies predicted from the model and the dashed lines represent the results from the FE software. (a), (b) and (c) represent the first three natural frequencies respectively.

3.5.2.2 Effect of Web thickness

Figure 3.12 shows the variation of natural frequencies of micro drill when the web thickness of increases from 10 to 20 percent of drill diameter, and other geometric parameters keep the same based on MD1 micro drill. It is observed that the first natural frequency increases by 25%

as the web thickness increases from 10% of the drill diameter to 20% of the drill diameter, whereas the variation of the second and third natural frequencies is less than 1%. The mode shapes for free-free condition of MD1 micro drill is shown in Figure 3.13. It can be observed that the first coupled mode is flute dominant, and the second vibration mode is shank and taper dominant. Therefore, with the increase in web thickness, the strength of the flute portion in torsional direction increases, and hence the first natural frequency increases. Whereas there is a minimal effect of Web thickness on the second natural frequency as the mode is dominated by the torsional vibration of the shank.

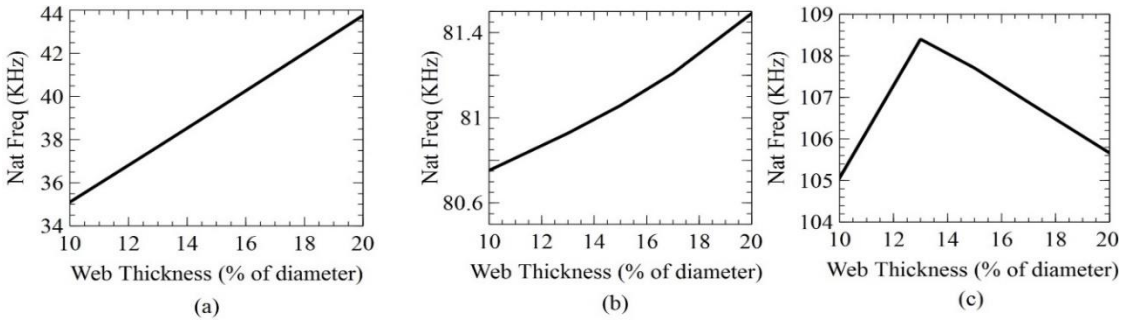

Figure 3.12 Variations of natural frequencies of the micro drill with web thickness. (a), (b) and (c) represent the first three natural frequencies respectively.

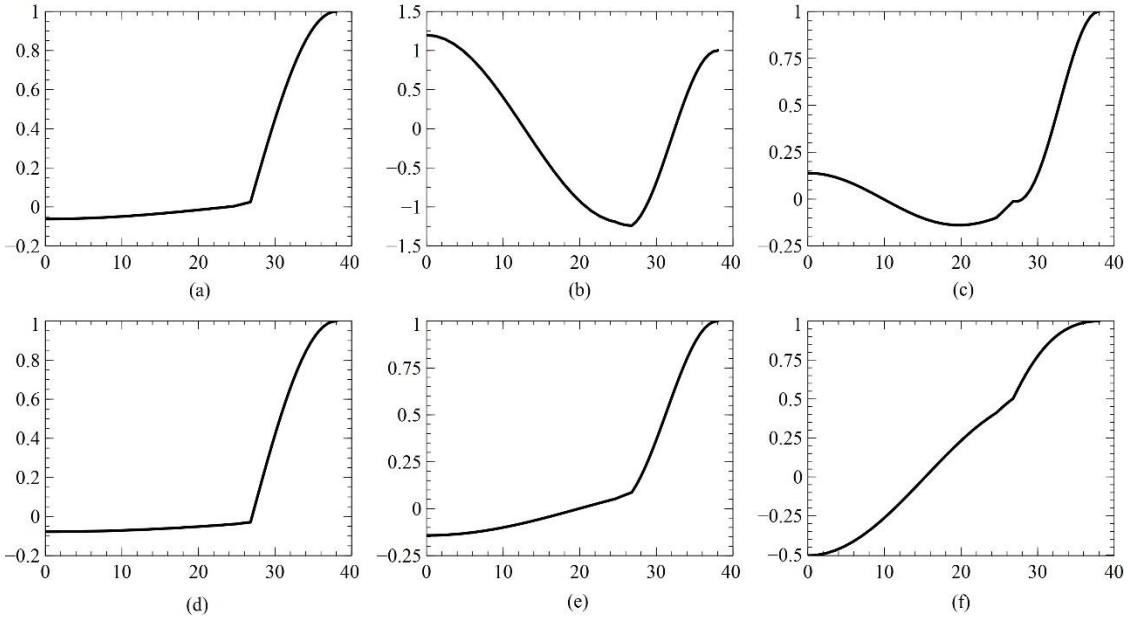

Figure 3.13 Predicted mode shape for MD1 micro drill geometry. (a), (b), (c) represent the first three axial modes, and (d), (e), (f) represent the first three torsional modes.

3.5.2.3 Effect of Aspect Ratio (AR)

In this study, the aspect ratio (l_3/d) of the flute section of the micro drill varies from 4 to 20 for MD1 micro drill geometry. The corresponding variations of the torsional-axial natural frequencies are presented in Figure 3.14. With the increase of the aspect ratio of the drill, the slenderness of the drilling tool increases, and consequently the natural frequencies decrease. It can be seen in Figure 3.14 that the first natural frequency decreases by 72%, second natural frequency decreases by 45% and the third natural frequency decreases by 53% as the aspect ratio increases from 5 to 20. The decrease rate of the natural frequency depends on the range of the aspect ratio. Hence, the critical value of aspect ratio of the drilling tool can be determined given the required natural frequency of the micro drill.

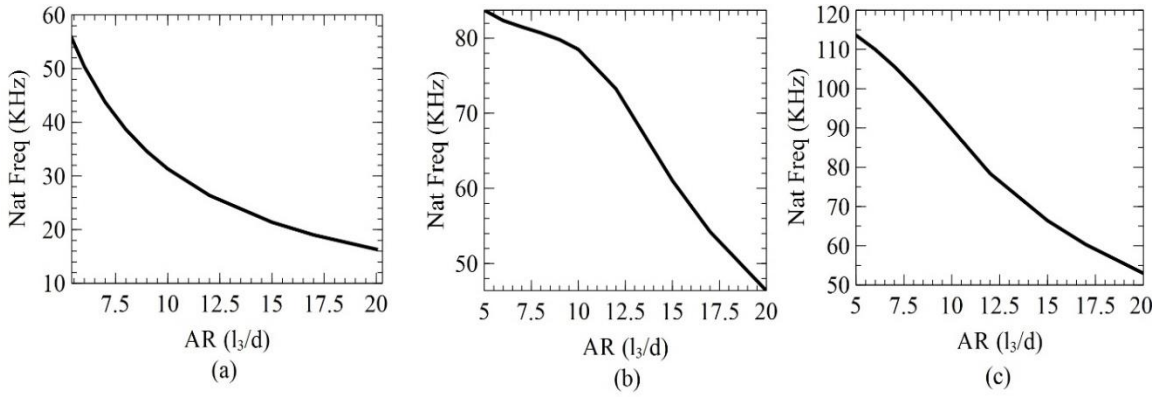

Figure 3.14 Variations of natural frequencies of micro drill with aspect ratio. (a), (b) and (c) represent the first three natural frequencies respectively.

3.6 Summary

A model based on 2D FE method is proposed to investigate the effect of warping deformation on the coupled torsional-axial vibration of the drilling tool. Warping constants for

general cross section shape of the drill are obtained, and the natural frequency and the mode shape corresponding to the torsional-axial dynamics are predicted. The predicted natural frequencies have less than 6% error compared to the results from commercial FE and experimental results, and the simulated results of the mode shapes match with the experiments. The computational efficiency is extensively improved based on the proposed model compared to the commercial FE software.

The effects of critical geometric parameters including helix angle, web thickness of the cross section and aspect ratio on the torsional-axial dynamics are quantitatively investigated for both conventional and micro drill. The variation of the natural frequency with respect to the geometric parameters depends on specific axial or torsional dominant vibration mode. The variation of the natural frequency is more obvious when the torsional dominant mode is involved, since it is mainly influenced by the warping constants than the axial dominant mode. Detailed analyses of the torsional-axial mode of the drilling tool based on the proposed model is able to provide an efficient way to select optimum geometric configuration of the drilling tool for required dynamic behavior.

CHAPTER IV

COUPLED TORSIONAL-AXIAL DYNAMICS OF DRILLING TOOL CONSIDERING CLAMPING BOUNDARY CONDITION

Receptance is defined by the ratio between steady state response of a structure and applied force (or torque). The receptances are used to determine the vibration dynamics of a structure depending on the direction of force and geometry of the structure. When a system contains more than one structure assembled together, dynamics of the combined system depends on the dynamics of each individual structure contained in it and the joint dynamics. The system is divided into a number of substructures and the receptance of each substructure is determined either analytically or experimentally, then the substructure receptances are coupled together using Receptance Coupling Substructure Analysis (RCSA) to predict the complete dynamics of the system. In a typical machining process, in order to predict the tool point response, analytical modeling of tool structure as a cantilever beam with completely fixed boundary condition is not sufficient as it fails to represent the actual boundary condition. The tool dynamics is highly influenced by the vibration modes of tool-holder, spindle head and machine structure. Furthermore, the dynamics at the clamped joint influences the dynamic displacement at tool tip. Hence, dynamics of spindle head and tool holder as well as joint dynamics need to be obtained in order to include the exact boundary condition.

In this thesis, a three-jaw chuck is used to investigate the effect of boundary condition on the drilling tool dynamics, shown in Figure 4.1. Classic receptance coupling technique is extended to predict torsional and axial receptances of the drilling tool considering the coupled torsional-axial vibration. Rigid and flexible receptance coupling techniques are used to predict the tool point dynamics. The simulation results are compared with experimental results, and the results are discussed in the following sections.

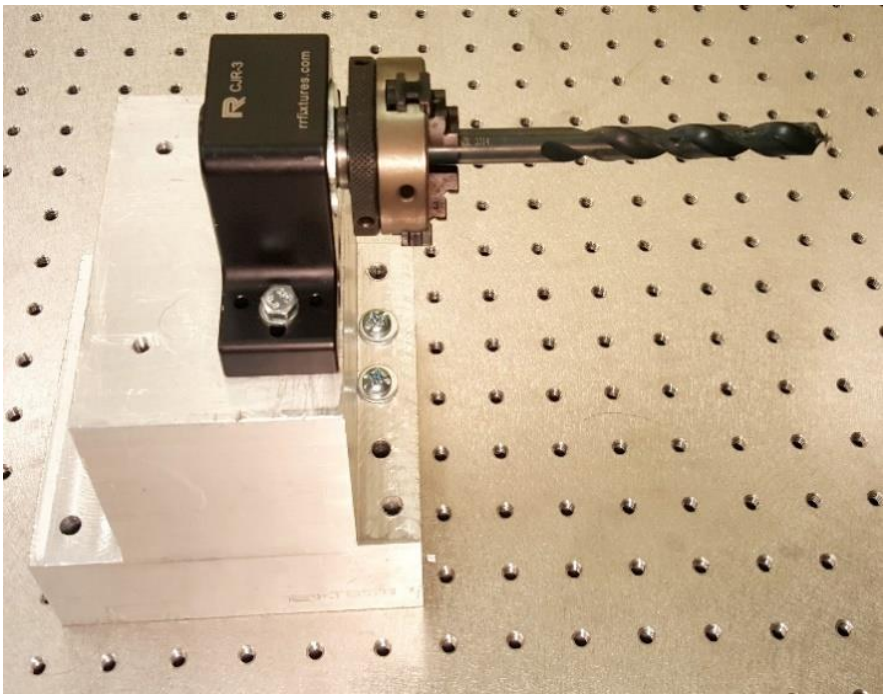

Figure 4.1 Drilling tool used for experiments fixed in a three-jaw chuck

4.1 Receptance coupling model of the drilling tool fixed in a three-jaw chuck

Although impact testing is normally applied at the tool point to determine the frequency response experimentally, it is a time-consuming process to conduct impact tests every time when the geometry or overhang of the tool change. In this thesis, the receptances of three-jaw chuck is determined through impact tests since its dynamics does not change, and the dynamics of drilling tool with varying geometry is obtained analytically as explained in chapter 3, RCSA method is

applied to predict the tool point response for the assembled structure, which includes both rigid receptance coupling and flexible receptance coupling.

4.1.1 Rigid Receptance coupling model with short blank tool

To apply rigid receptance coupling model for torsional-axial dynamics, the drilling tool is cut into two pieces as shown in Figure 4.2. The whole system is divided into two substructures, with the chuck and fixture along with the short shank portion of the drill considered as Substructure B, and the remaining portion of the tool is considered as Substructure A. The end points for each substructure 1, 2a and 2b are marked as shown in Figure 4.3.

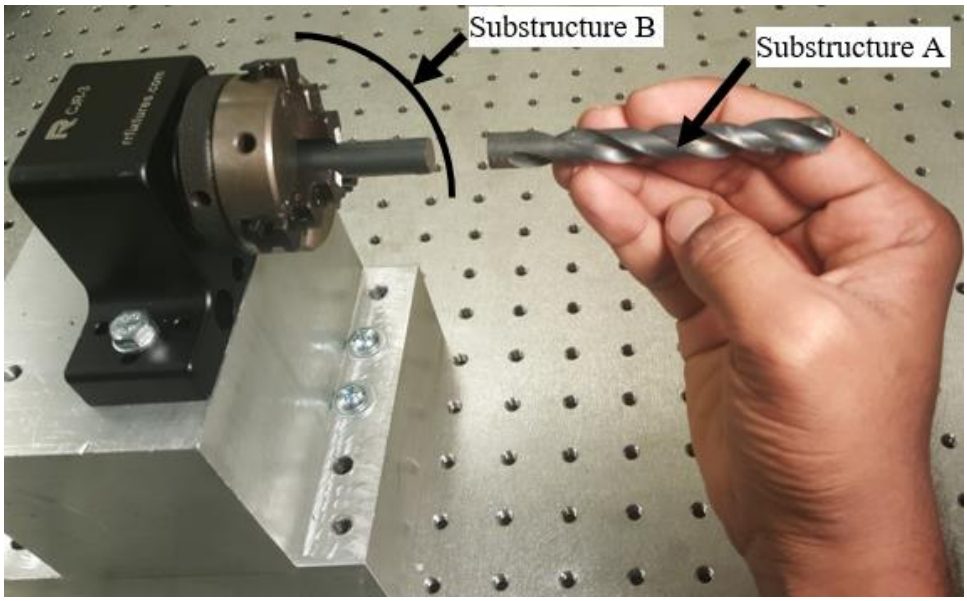

Figure 4.2 Figure showing the substructures used for rigid receptance coupling

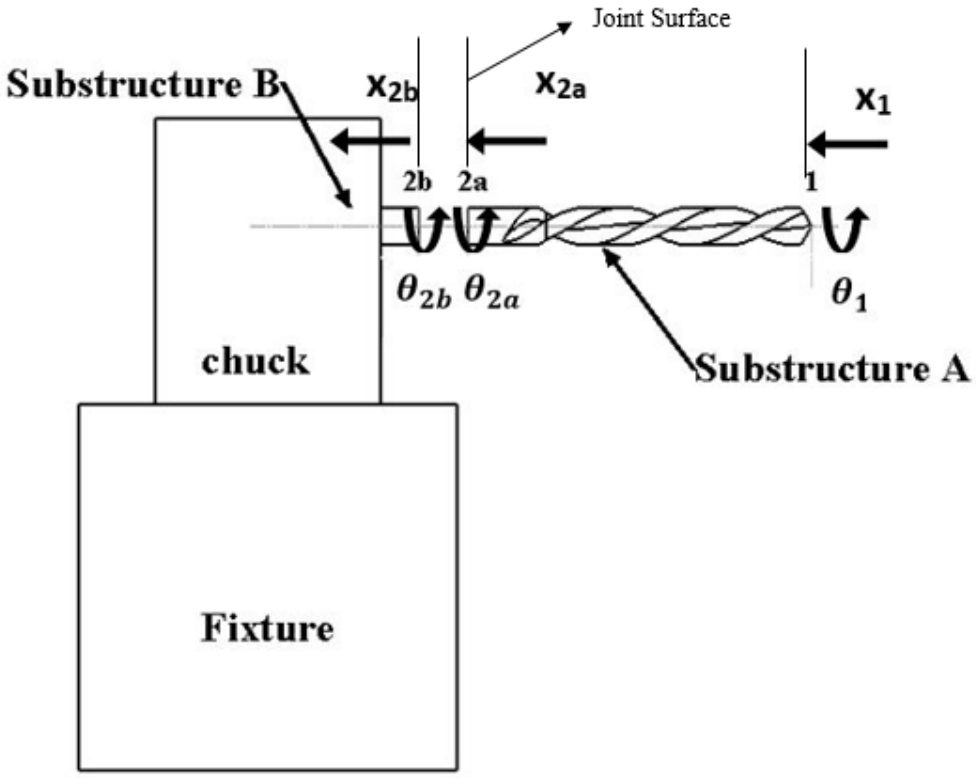

Figure 4.3 Rigid receptance coupling model

In Figure 4.3, x_1, x_{2a}, and x_{2b} are the coordinates defining the axial responses and $\theta_1, \theta_{2a}, \theta_{2b}$ are the coordinates defining the torsional responses at points 1, 2a and 2b respectively. a_1, a_{2a}, and a_{2b} are the axial forces applied, and t_1, t_{2a}, and t_{2b} are the torsional moments acting at the three locations. Therefore, the direct receptances at point 1 are:

$$h_{11,aa} = \frac{x_1}{a_1}, h_{11,at} = \frac{x_1}{t_1}, h_{11,ta} = \frac{\theta_1}{a_1}, h_{11,tt} = \frac{\theta_1}{t_1} \; and \; [h_{11}] = \begin{bmatrix} h_{11,aa} & h_{11,at} \\ h_{11,ta} & h_{11,tt} \end{bmatrix} \tag{4.1}$$

The cross receptances at point 1 are:

$$h_{12a,aa} = \frac{x_1}{a_{2a}}, h_{12a,at} = \frac{x_1}{t_{2a}}, h_{12a,ta} = \frac{\theta_1}{a_{2a}}, h_{12a,tt} = \frac{\theta_1}{t_{2a}} \; and$$

$$[h_{12a}] = \begin{bmatrix} h_{12a,aa} & h_{12a,at} \\ h_{12a,ta} & h_{12a,tt} \end{bmatrix} \tag{4.2}$$

The direct receptances at point 2a are:

$$h_{2a2a,aa} = \frac{x_{2a}}{a_{2a}}, h_{2a2a,at} = \frac{x_{2a}}{t_{2a}}, h_{2a2a,ta} = \frac{\theta_{2a}}{a_{2a}}, h_{2a2a,tt} = \frac{\theta_{2a}}{t_{2a}} \; and$$

$$[h_{2a2a}] = \begin{bmatrix} h_{2a2a,aa} & h_{2a2a,at} \\ h_{2a2a,ta} & h_{2a2a,tt} \end{bmatrix} \tag{4.3}$$

The cross receptances at point 2a are:

$$h_{2a1,aa} = \frac{x_{2a}}{a_1}, h_{2a1,at} = \frac{x_{2a}}{t_1}, h_{2a1,ta} = \frac{\theta_{2a}}{a_1}, h_{2a1,tt} = \frac{\theta_{2a}}{t_1} \; and$$

$$[h_{2a1}] = \begin{bmatrix} h_{2a1,aa} & h_{2a1,at} \\ h_{2a1,ta} & h_{2a1,tt} \end{bmatrix} \tag{4.4}$$

The direct receptances at the joint location 2b are:

$$h_{2b2b,aa} = \frac{x_{2b}}{a_{2b}}, h_{2b2b,at} = \frac{x_{2b}}{a_{2b}}, h_{2b2b,ta} = \frac{\theta_{2b}}{a_{2b}}, h_{2b2b,tt} = \frac{\theta_{2b}}{t_{2b}} and$$

$$[h_{2b2b}] = \begin{bmatrix} h_{2b2b,aa} & h_{2b2b,at} \\ h_{2b2b,ta} & h_{2b2b,tt} \end{bmatrix} \tag{4.5}$$

Equations 4.1 to 4.5 represent the individual component receptances that form the assembly structure. These receptances can be conveniently written in generalized matrix form as:

$$\begin{Bmatrix} x_i \\ \theta_i \end{Bmatrix} = [h_{ij}] \begin{Bmatrix} f_j \\ m_j \end{Bmatrix} \rightarrow \{u_i\} = [h_{ij}]\{q_j\} \tag{4.6}$$

where h_{ij} is the generalized receptance matrix with response at point *i* and excitation and response at *j* ($i, j = 1, 2a, 2b$) and u_i and q_j are generalized response and excitation matrices.

The component receptances for substructure A and substructure B using the above notations are written as:

$$u_1 = h_{11}q_1 + h_{12a}q_{2a} \text{ and } u_{2a} = h_{2a1}q_1 + h_{2a2a}q_{2a} \quad (4.7a)$$

$$u_{2b} = h_{2b2b}q_{2b} \quad (4.7b)$$

The two substructures A and B are then combined to form an assembly as shown in Figure 4.4.

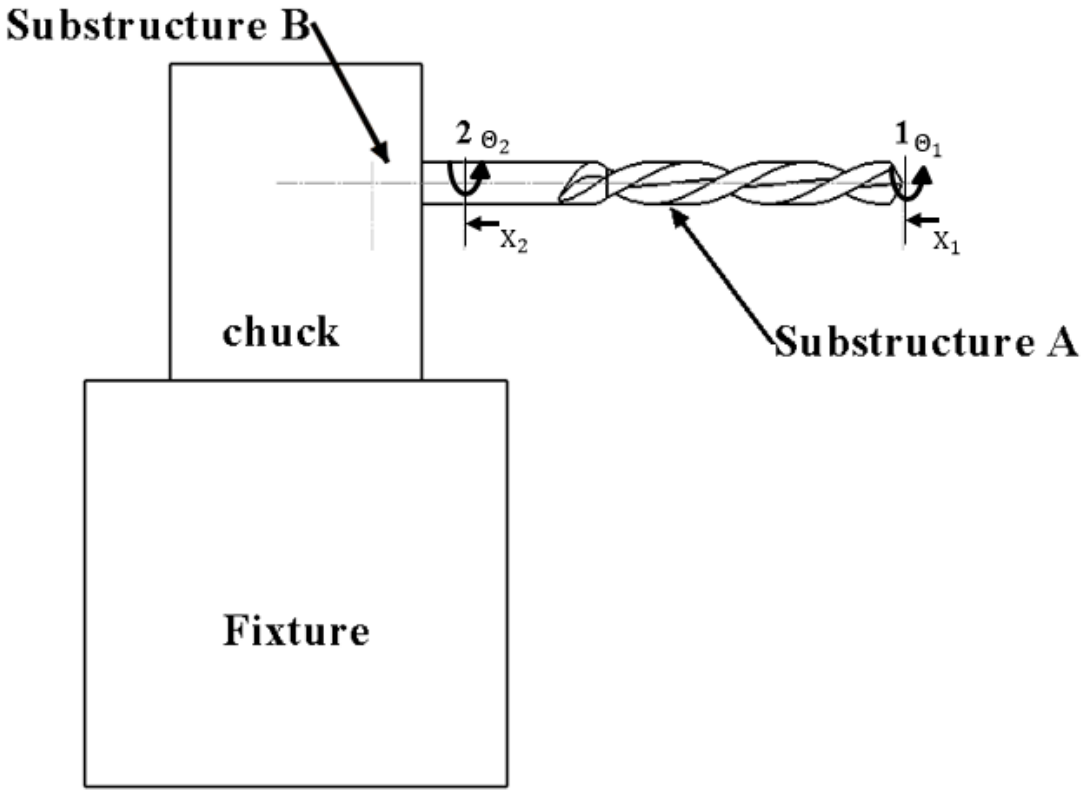

Figure 4.4 Rigid Receptance Coupling of the two substructures to form assembly.

The generalized form for the assembly receptances is expressed as:

$$\begin{Bmatrix} U_1 \\ U_2 \end{Bmatrix} = \begin{bmatrix} H_{11} & H_{12} \\ H_{21} & H_{22} \end{bmatrix} \begin{Bmatrix} Q_1 \\ Q_2 \end{Bmatrix} \quad (4.8)$$

where $U_i = \begin{Bmatrix} X_i \\ \Theta_i \end{Bmatrix}, H_{ij} = \begin{bmatrix} H_{ij,aa} & H_{ij,at} \\ H_{ij,ta} & H_{ij,tt} \end{bmatrix}$ *and* $Q_j = \begin{Bmatrix} A_j \\ \mathrm{T}_j \end{Bmatrix}$

The compatibility conditions for the assembled structure that represent the rigid coupling between substructure A and substructure B at point 2 is:

$$u_{2b} - u_{2a} = 0 \rightarrow u_{2b}{=}u_{2a}{=}U_2 \quad \text{and} \quad u_1 = U_1 \tag{4.9}$$

The equilibrium conditions for the assembled structure to equate the internal and external forces are:

$$q_{2a} + q_{2b} = 0 \; and \; q_1 = Q_1 \tag{4.10}$$

Based on the compatibility and equilibrium conditions in rigid receptance coupling, the FRFs of the assembled structure at point 1 are given as [11]:

$$[H_{11}] = [h_{11}] \; - [h_{12a}] \; ([h_{2a2a}] + [h_{2b2b}])^{-1} [h_{12a}] \tag{4.11}$$

$$[H_{21}] = [h_{2a1}] - [h_{2a2a}] \; ([h_{2a2a}] + [h_{2b2b}])^{-1} [h_{2a1}] \tag{4.12}$$

And the direct and cross FRFs at point 2 are:

$$[H_{22}] = \frac{U_2}{Q_2} = [h_{2a2a}] - [h_{2a2a}] \; ([h_{2a2a}] + [h_{2b2b}])^{-1} [h_{2a2a}] \tag{4.13}$$

$$[H_{12}] = \frac{U_1}{Q_2} = [h_{12a}] - [h_{12a}] ([h_{2a2a}] + [h_{2b2b}])^{-1} [h_{2a2a}] \tag{4.14}$$

In the Equations 4.11 through 4.14, the receptance matrices corresponding to substructure A are determined analytically using the model developed in chapter 3. The unit for all the receptances from the model is considered to be m/N for the magnitude so as to maintain consistency with the experimental receptances. The first two modes of the drilling tool corresponding to the free-free boundary condition of the tool are considered and a constant modal damping ratio of 0.12% which is experimentally obtained for free-free boundary condition is considered for both the modes. Figure 4.5– Figure 4.7 show the direct and cross receptances of Substructure A.

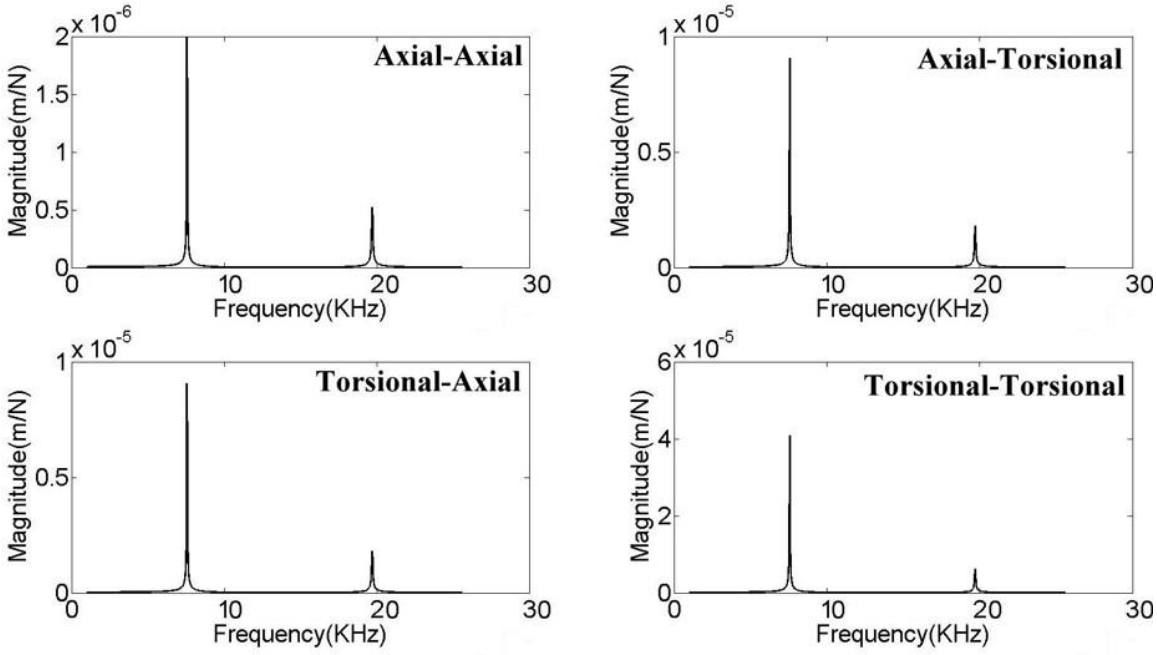

Figure 4.5 Predicted free-free receptances of substructure A when excitation is at point 1 and response is predicted at point 1.

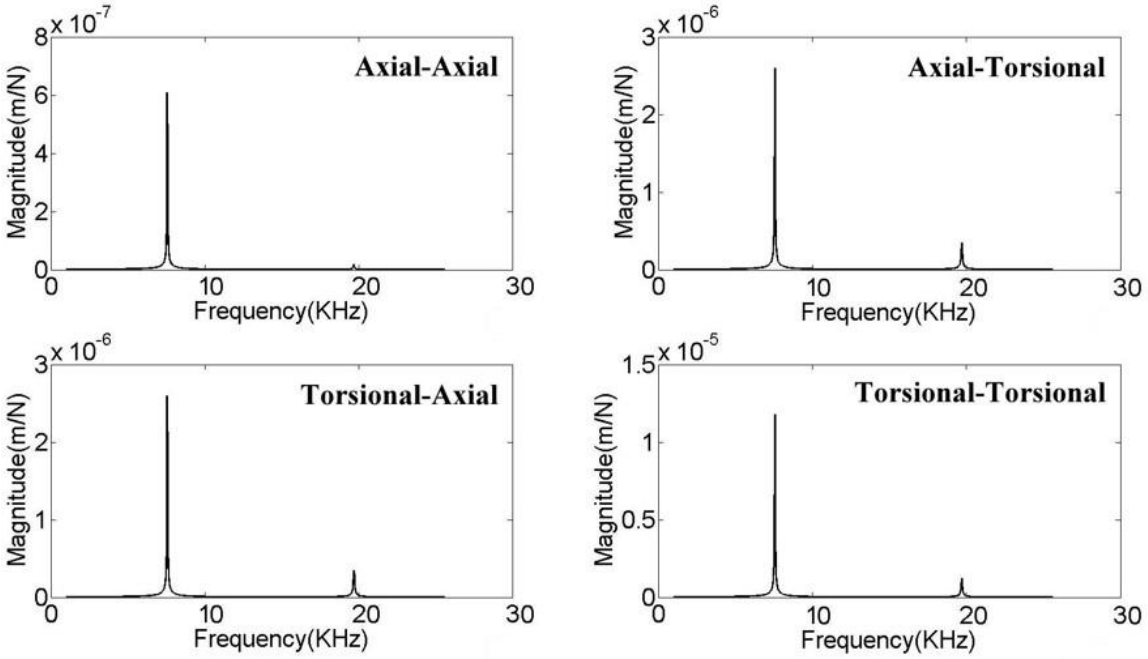

Figure 4.6 Predicted free-free receptances of substructure A when excitation is at point 1 and response is predicted at point 2a.

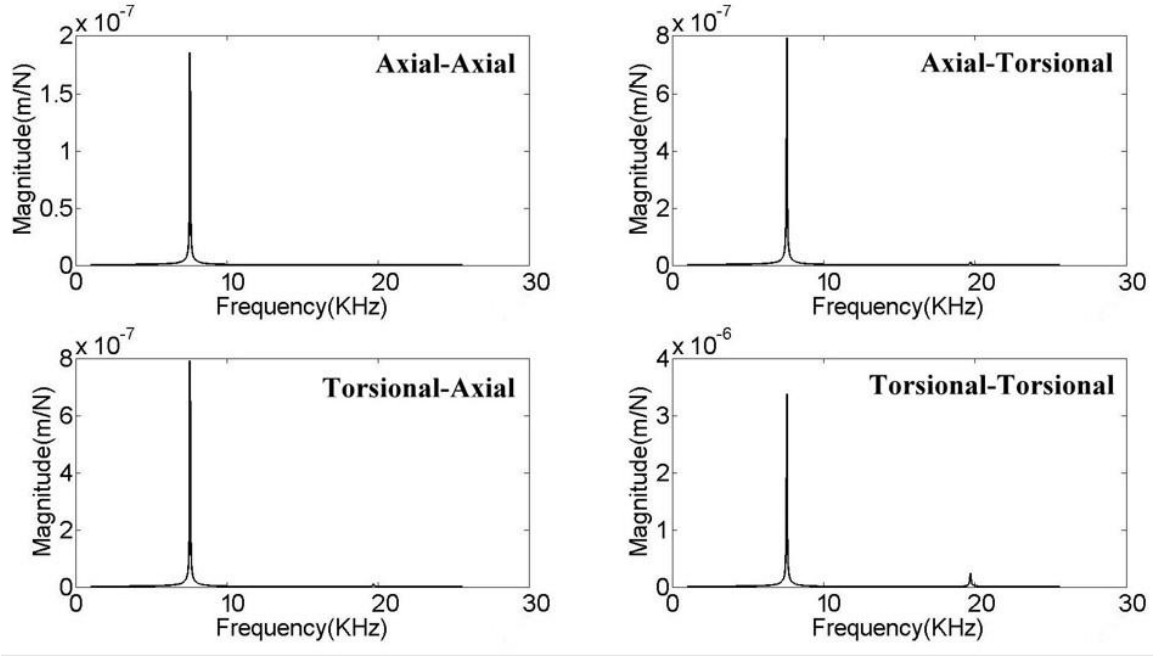

Figure 4.7 Predicted free-free receptances of substructure A when excitation is at point 2a and response is predicted at point 2a.

4.1.2 Identification of joint dynamics using flexible receptance coupling model

In rigid Receptance coupling model, the tool is cut into two pieces with a small portion of the shank part fixed in the three-jaw chuck and considered as substructure B. This approach will be useful when analyzing the dynamics of micro drilling tool. Generally, micro drilling tools have the same shank portion for different diameters of the flute portion. The taper part of the micro drill acts as a connection from shank portion to flute portion. In such a case, the dynamics of different tools can be still analyzed with same blank tool in the chuck. Whereas in conventional drilling tools, the size of the shank is the same as the size of flute portion and diameter of the short blank tool changes with different tools. This requires experimental identification of dynamics for each shank of each drill which may be time consuming. In such a case, the drilling tool as a whole is considered as substructure A with chuck and fixture (without the short blank tool) as substructure B as shown in Figure 4.8. The analytical FRFs of drilling tool as a whole are predicted and coupled

to the machine tool spindle holder by a joint with finite stiffness and damping parameters as shown in Figure 4.9.

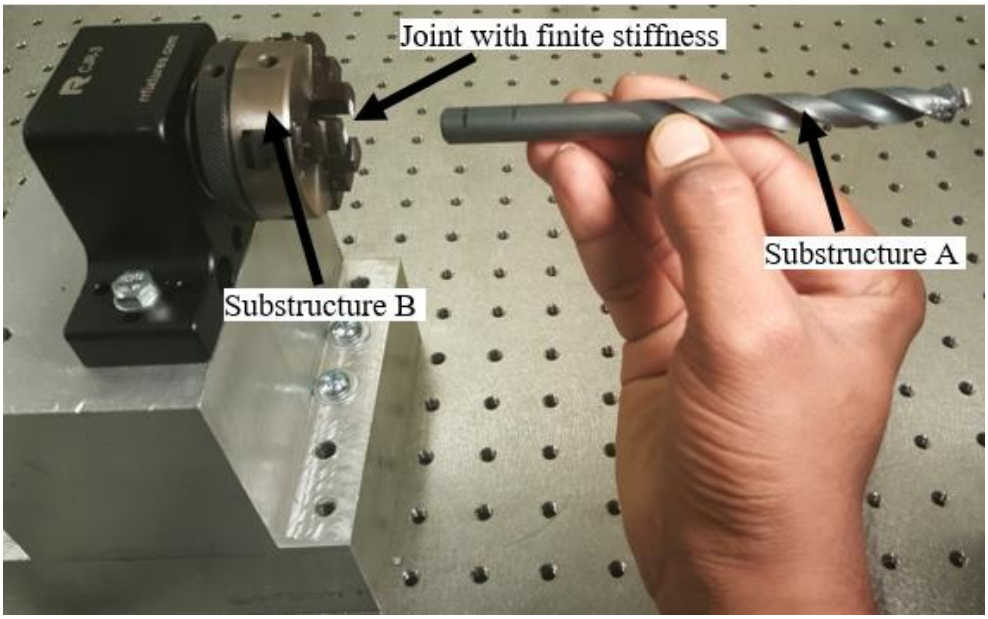

Figure 4.8 Substructures and joint for flexible receptance coupling

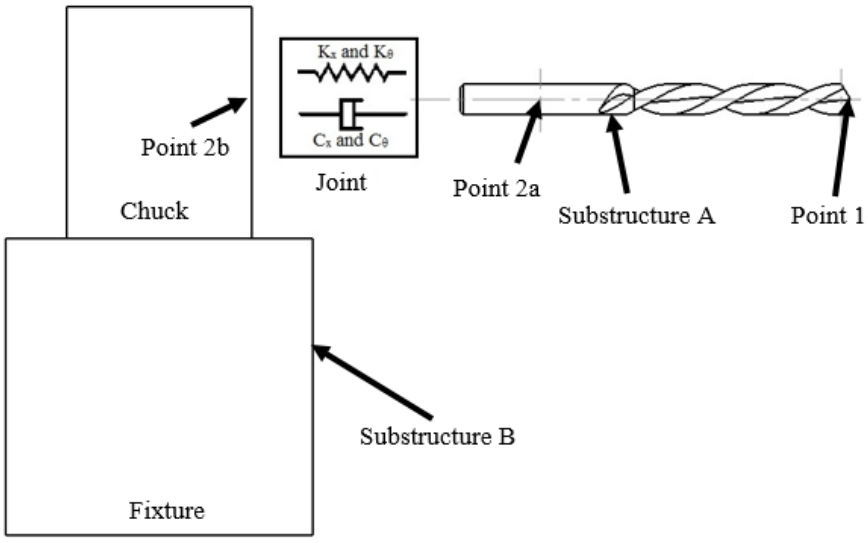

Figure 4.9 Flexible Receptance coupling model

The drilling tool is connected to the chuck at point 2a. Hence, in the assembled system, point 2b and point 2a are connected by a joint with stiffness parameters being K_x and K_θ and damping parameters being C_x and C_θ in axial and torsional directions respectively. When force is applied at point 1 and responses are predicted at points 2a and 1, the cross and direct FRFs are [47, 58]:

$$[H_{11}] = [h_{11}] - [h_{12a}]\,[h_2]^{-1}[h_{12a}] \tag{4.15}$$

$$[H_{21}] = [h_{2a1}] - [h_{2a2a}]\,[h_2]^{-1}[h_{2a1}] \tag{4.16}$$

where $[h_2] = [h_{2a2a}] + [h_{2b2b}] + [h_J]$, $[h_{2b2b}]$ is the receptance matrix for substructure B at point 2b and $[h_J]$ is the receptance matrix of the joint surface. Similarly, when a force is applied at point 2 of the assembled structure, the cross and direct FRFs with joint dynamics are given as:

$$[H_{22}] = [h_{2a2a}] - [h_{2a2a}]\,[h_2]^{-1}[h_{2a2a}] \tag{4.17}$$

$$[H_{12}] = [h_{12a}] - [h_{12a}][h_2]^{-1}[h_{2a2a}] \tag{4.18}$$

In Equations 4.15 through 4.18, the receptance matrices corresponding to the drill can be modelled using the model proposed in chapter 3. $[h_{2b2b}]$ and $[h_J]$ are constant once modeled for the same chuck with the same boundary conditions. Hence, modeling of $[h_{2b2b}]$ and $[h_J]$ together will facilitate the calibration of joint dynamics in predicting the drilling tool dynamics. The receptances corresponding to axial degrees of freedom in Equations 4.15 through 4.18 are obtained by impact experiments and the receptance matrix $[h_2]$ is predicted by extracting the first elements from the matrices given in Equations 4.15, 4.17 and 4.19. To facilitate the derivation, the receptance symbols are simplified as: $h_{11,aa} = a,\ h_{12,aa} = b,\ h_{22,aa} = c, h_{12,at} = d, h_{22,at} = e, h_{22,tt} = f, H_{11,aa} = k, H_{12,aa} = l, H_{22,aa} = m,\ h_{2,aa} = x, h_{2,at} = y = h_{2,ta}, h_{2,tt} = z.$

Hence, the matrix $[h_2] = \begin{bmatrix} x & y \\ y & z \end{bmatrix}$ can be predicted as:

$$x = \frac{b^2c - ac^2 + c^2k - 2bcl + b^2m}{b^2 - ac + ck - 2bl + l^2 + am - km} \tag{4.19a}$$

$$y = \frac{b^2e - ace + cek - cdl - bel + bdm}{b^2 - ac + ck - 2bl + l^2 + am - km} \tag{4.19b}$$

$$z = \frac{-cd^2 + 2bde - ae^2 + e^2k - 2del + d^2m}{b^2 - ac + ck - 2bl + l^2 + am - km} \tag{4.19c}$$

The receptance matrix which is a combination of joint receptances and substructure B receptances need to be calculated and kept constant for the same chuck and same boundary conditions.

$$[h_{2b2b}] + [h_J] = \begin{bmatrix} x - h_{2a2a,aa} & y - h_{2a2a,at} \\ y - h_{2a2a,ta} & z - h_{2a2a,tt} \end{bmatrix} \tag{4.20}$$

The receptance matrices corresponding to several conventional drilling tools are predicted analytically and can be directly coupled to form an assembly using Equation 4.20, therefore the complete dynamics of the assembled structure are predicted.

4.2 Experimental Results and Analysis

4.2.1 Results for rigid receptance coupling with short blank tool

Experiments are conducted to obtain the receptances at the tip of substructure B to use in receptance coupling technique, and also to obtain the receptances at the tool tip for the validation of the simulation results. The experimental setup using the LDV-hammer tests is the same as that discussed in chapter 3. Figure 4.10 shows the setup for determining the four receptances corresponding to the torsional-axial vibration at the tip of the drilling tool.

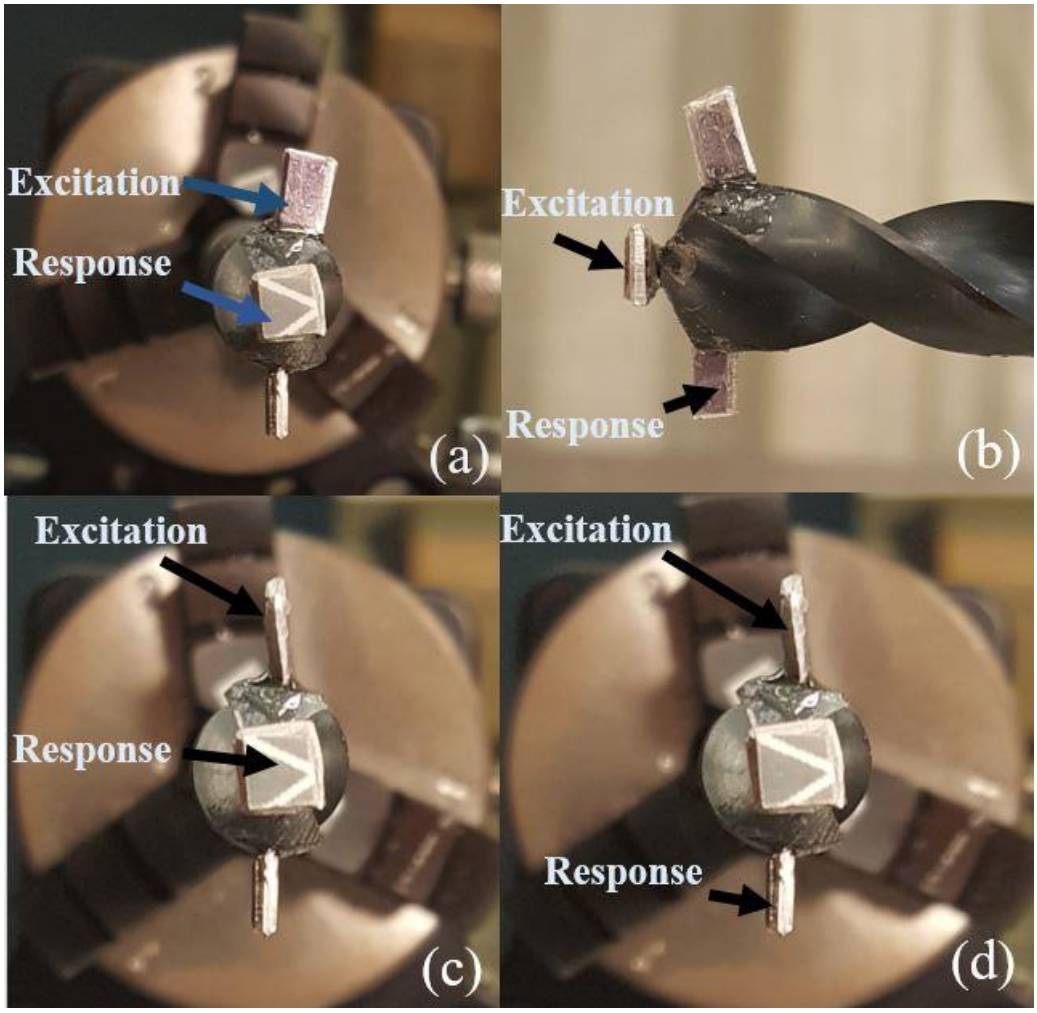

Figure 4.10 Measurement procedure with small plate attached to the drilling tool (a) Axial-Axial (b) Axial-Torsional (c) Torsional-Axial (d) Torsional-Torsional

While performing the experiment, it is impossible to provide exact axial excitation using an impact hammer and also the plate A may not be attached exactly perpendicular to the laser beam. Because of these uncertainties in the experiment, some of the bending modes are excited and the FRF is a mixture of bending-axial-torsional vibration mode. Hence, a setup shown as Figure 4.11 is developed to identify the bending modes. Two plates are attached as shown in Figure 4.10 (d) to make the torsional-torsional measurement. Two measurements are to be made in order to eliminate the bending modes from the FRF. First experiment is conducted by excitation given on plate A and

response is measure on the same plate. Second experiment is conducted by exciting the beam in opposite direction on plate B as shown in Figure 4.11 and response is measured at the same location as that of the first experiment. This reverses the bending direction keeping the torsion direction to be same. Hence in the FRF it can be clearly seen that the peaks of imaginary parts corresponding to bending modes reverse their direction as shown in Figure 4.12.

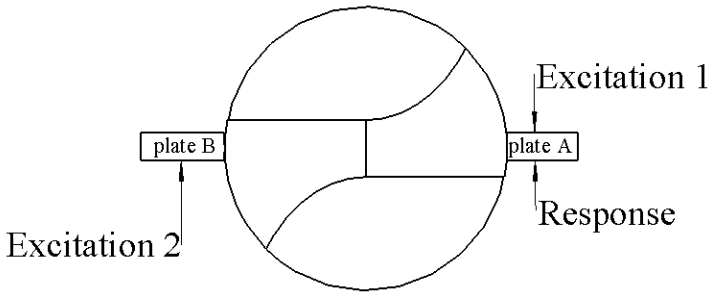

Figure 4.11 Schematic of measurement made for tool tip's torsional-torsional FRF.

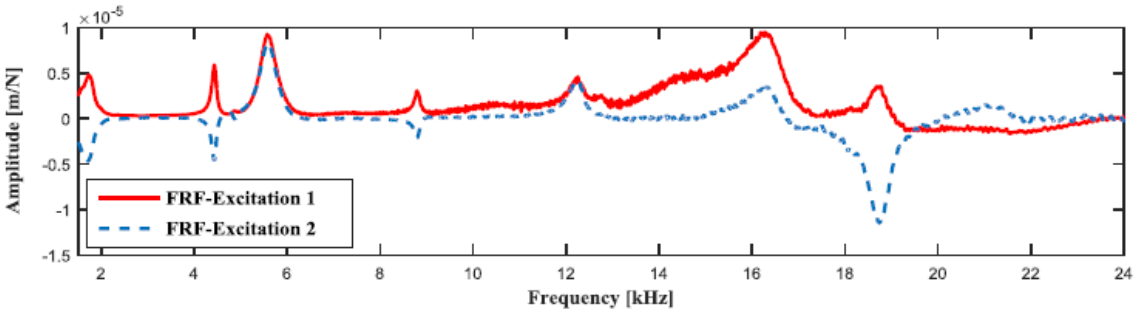

Figure 4.12 FRFs comparison showing the reversal of bending modes measured by CutPro.

The same bending modes can be identified from other FRFs given in Figure 4.10, and the FRFs for bending modes are separated from the torsional-axial modes. Using this method, experimental FRFs are determined at the tip of substructure B and also at the tool tip. Figure 4.13 shows the experimentally determined receptances when Substructure B is excited at point 2b and the response is measured at point 2b ($[h_{2b2b}]$). Based on Equation (4.11), rigid receptance coupling is applied for the two substructures and the receptance of the assembled structure is predicted. To

validate the results, modal experiments are conducted on the fixture-holder-drilling tool assembly and the required torsional-axial modes are extracted from the FRF as shown in Figure 4.14. The comparison is conducted between the predicted results and the measurement results, as shown in Figure 16. The values of the natural frequencies and the peak values of the FRFs are listed in Table 3. The FRF of the drilling tool based on a cantilever beam assumption is also obtained and shown in Figure 16. It can be observed that the proposed receptance coupling model predicts the complete dynamics of drilling tool with a satisfactory agreement to the measured dynamics. The first tool mode is found closer to 5.6 KHz. Other peaks are observed resulting from the substructure B. A major difference of natural frequency and peak magnitude of the FRFs is observed based on the comparison of cantilever beam approximation and the experiments. Hence, the dynamics of the supporting structure and the clamping boundary condition influence the overall coupled-axial receptance at the tool tip, and the proposed RC model is able to effectively predict the corresponding dynamic behavior of the drilling tool. Based on the natural frequencies listed in Table 3, the modes at 5.6 kHz, 12 kHz and 16 kHz are from the torsional-axial vibration of the drilling tool, since the peaks appear in both the axial-torsional and torsional-torsional plots in Figure 16. The reason that 12 kHz and 16 kHz are not shown in axial-axial plot is probably due to the high rigidity in axial direction. The modes at 9.4 kHz and 14.7 kHz are attributed to the deformation of the fixture, since they only influence the axial-axial FRF. Further, the FRF plots in Figure 16 show that the torsional-axial mode of drilling tool at 5.6 kHz has the highest peak, which is the dominant mode influencing chatter stability.

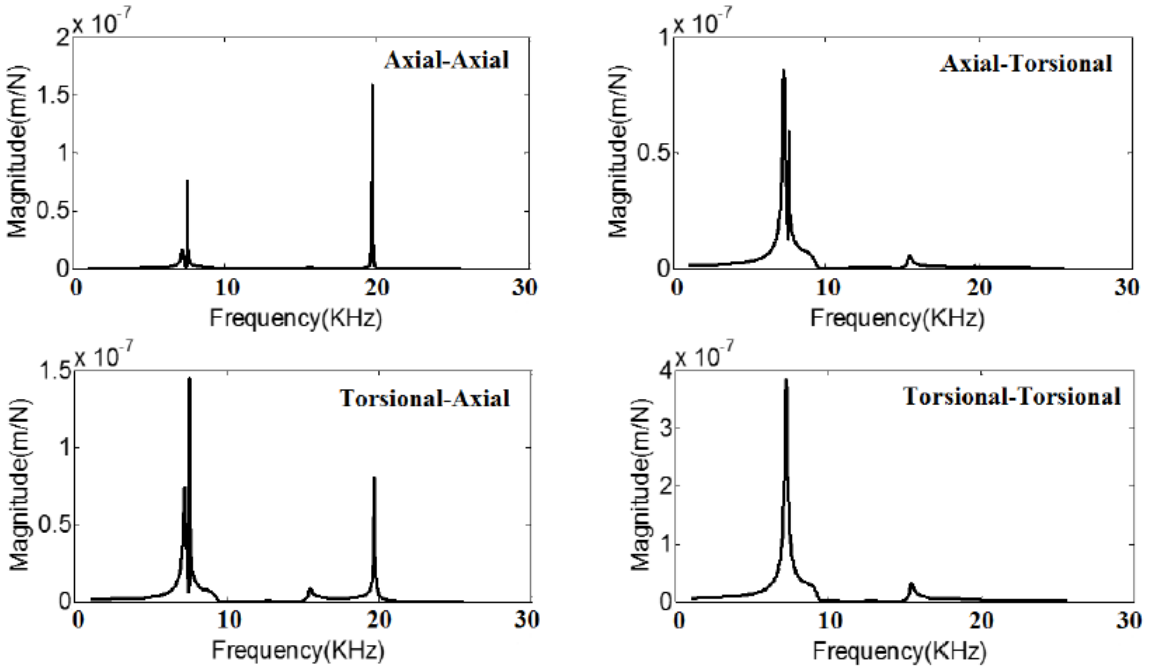

Figure 4.13 Magnitude FRFs for the Substructure B

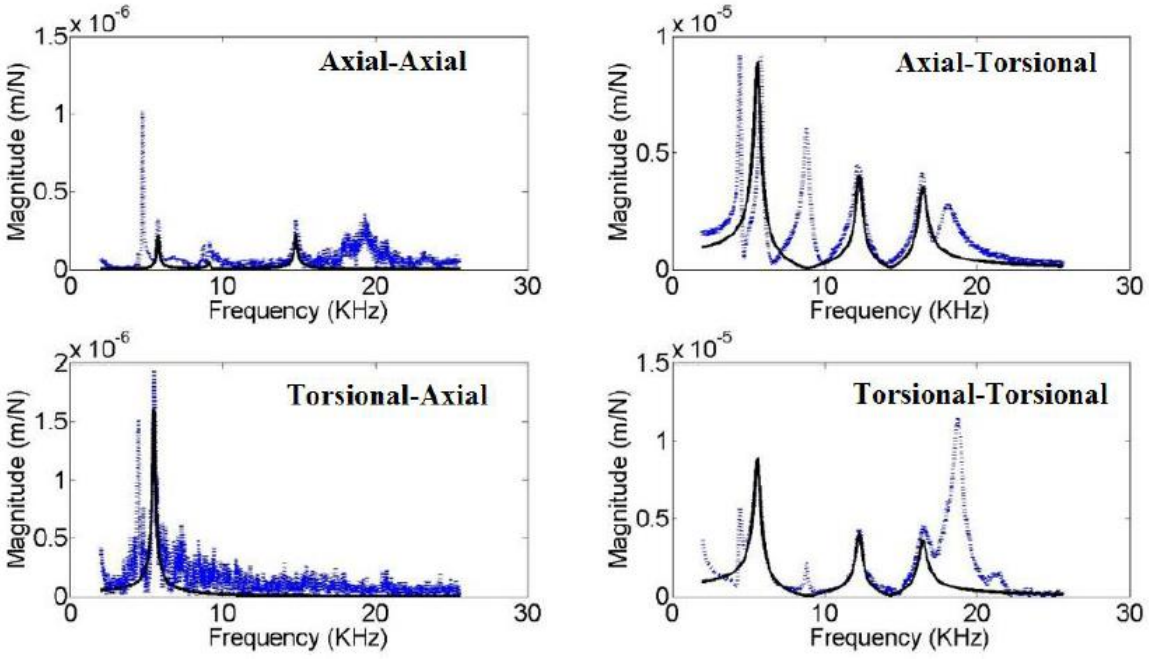

Figure 4.14 Extraction of torsional-axial modes from the experimental data

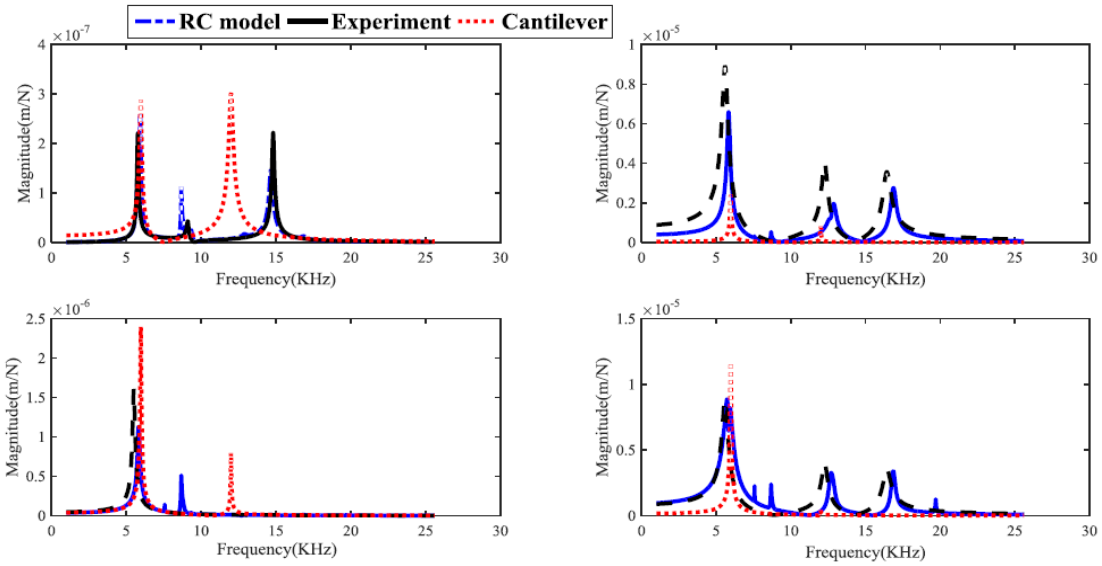

Figure 4.14 Predicted vs Measured FRF at the Tool tip using rigid receptance coupling.

Table 4.1 Comparison of Natural frequencies and Magnitude peaks between measured and predicted FRFs when rigid receptance coupling is used.

Type of vibration	Mode	Natural Frequencies(Hz)			Peaks (m/N)		
		Exp	RC	%	Exp	RC	%
Axial-axial	1	5770	5890	-2.07972	2.21E-07	2.22E-07	-0.67904
	2	9100	9360	-2.85714	4.30E-08	2.91E-08	32.28585
	3	14813	14660	1.032877	2.22E-07	2.23E-07	-0.45005
Axial-Torsional	1	5590	5830	-4.29338	8.90E-06	7.55E-06	15.23082
	2	12250	12830	-4.73469	4.02E-06	2.10E-06	47.63446
	3	16410	16860	-2.74223	3.56E-06	2.78E-06	21.83811
Torsional-Axial	1	5580	5820	-4.30108	1.61E-06	1.28E-06	20.31153
Torsional-Torsional	1	5590	5820	-4.11449	8.90E-06	1.19E-05	-33.7751
	2	12260	12680	-3.42577	4.02E-06	3.18E-06	20.85508
	3	16430	16850	-2.5563	3.26E-06	2.24E-06	31.40319

4.2.2 Results for flexible receptance coupling with identification of joint dynamics

For the identification of joint dynamics, the FRFs corresponding to axial vibration of the drilling tool must be measured from the experiments. Setup for Modal testing on the drilling tool attached in three-jaw chuck is shown in Figure 4.15. D1 drilling tool as shown in Table 3.2 is used for the calibration of joint dynamics. Point 1 is located at the tip of the drilling tool and point 2 is located near the chuck-tool interface. Three experiments were conducted on the drilling tool to obtain direct and cross axial-axial FRFs at points 1 and 2, including $H_{11,aa}$, $H_{22,aa}$ and $H_{12,aa}$. Other FRFs in Equations 4.19 are predicted from the model proposed in chapter 3. Hence, using Equations 4.19 and 4.20 the receptance matrices corresponding to joint dynamics are identified as shown in Figure 4.16.

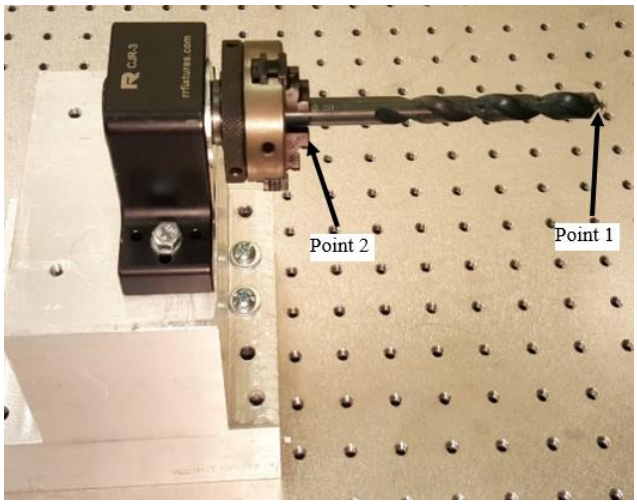

Figure 4.15 Setup for modal testing on drilling tool for identification of joint dynamics

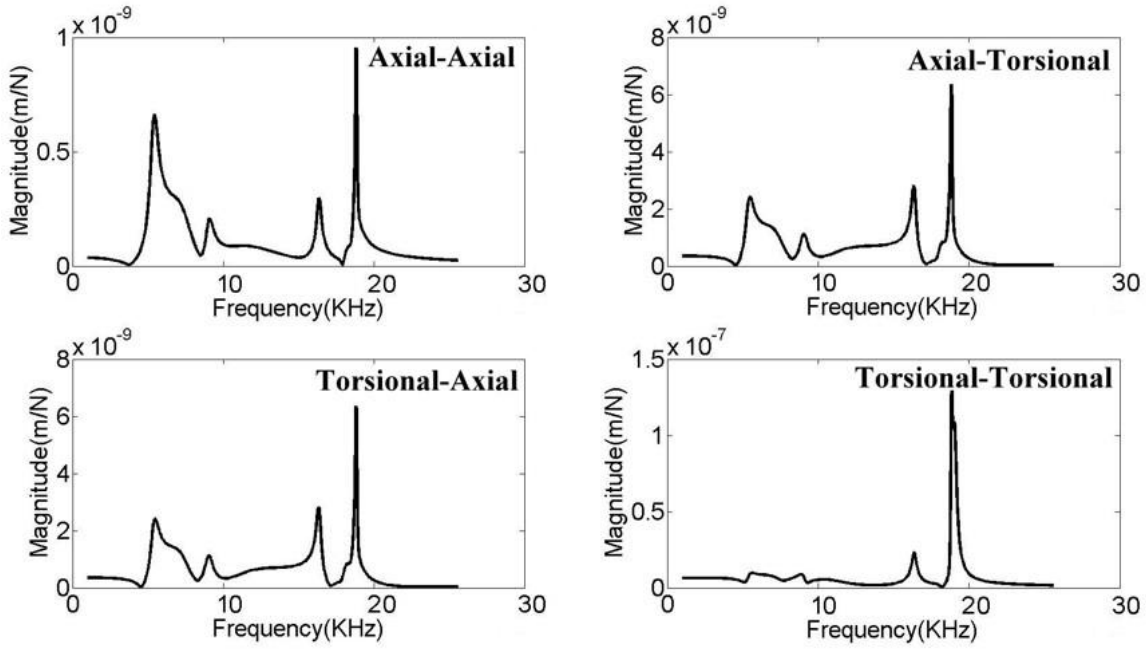

Figure 4.16 FRFs for the three-jaw chuck along with joint dynamics

To validate the above determined joint dynamics a 15mm diameter drilling tool with 30^0 helix angle and an overall length of 168 mm is selected with same material as the D1 drilling tool. Tip FRFs for this drilling tool are predicted using the identified joint dynamics and Equation 4.15. The predicted FRFs are validated through experimentally measured FRFs.

The comparison of natural frequencies and peak magnitudes of the FRFs when flexible receptance coupling model is applied are shown in Figure 4.17 and numerical values are tabulated in Table 4.2. It is observed from Figure 4.17 and Table 4.2 that the proposed receptance coupling model predicts the natural frequencies of drilling tool with joint dynamics with a satisfactory agreement to the measured dynamics. The errors in the comparison are due to complex non-linear damping present near the joint which was not modeled in the RC technique.

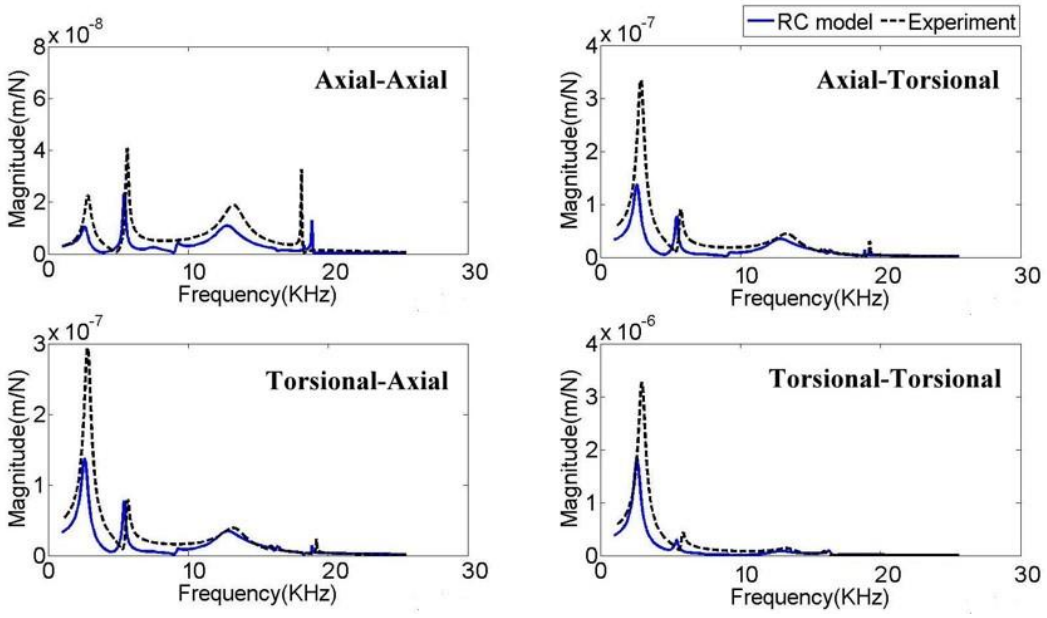

Figure 4.17 Predicted vs measured FRFS at the tool tip using flexible receptance coupling.

Table 4.2 Comparison of natural frequencies and magnitude peaks between measured and predicted FRFs when flexible receptance coupling is used.

Type of vibration	Mode	Natural Frequencies(Hz)			Peaks (m/N)		
		Exp	RC	% error	Exp	RC	% error
Axial-axial	1	2830	2580	8.8	2.3E-08	1.1E-08	53.3
	2	5780	5440	5.9	5.1E-08	2.4E-08	53.4
	3	13270	12750	3.9	1.9E-08	1.1E-08	42.2
	4	20060	18860	6.0	3.3E-08	1.3E-08	60.2
Axial-Torsional	1	2890	2600	10.0	3.3E-07	1.4E-07	58.8
	2	5830	5440	6.7	1.1E-07	7.8E-08	31.1
	3	13290	12810	3.6	4.4E-08	3.5E-08	21.5
	4	15830	16390	-3.5	2.2E-08	1.3E-08	40.6
	5	19220	18860	1.9	3.0E-08	1.4E-08	53.0
Torsional-Axial	1	2810	2590	7.8	2.9E-07	1.4E-07	53.3
	2	5780	5430	6.1	1.1E-07	7.6E-08	27.5

	3	13250	12760	3.7	3.9E-08	3.5E-08	10.4
	4	20010	18860	5.7	4.4E-08	1.4E-08	68.1
Torsional-Torsional	1	2960	2600	12.2	3.3E-06	1.8E-06	44.5
	2	13260	12850	3.1	1.4E-07	8.6E-08	38.6
	3	15970	16320	-2.2	8.4E-08	8.9E-08	-6.1

4.3 Summary

An enhanced receptance coupling technique that can be used to predict torsional-axial vibrations of drilling tool is proposed. Both rigid and flexible receptance coupling models are used to predict the tool tip dynamics of drilling tool fixed in a three-jaw chuck. The dynamics of the chuck are obtained through modal measurements, and the dynamics of the drilling tool are predicted numerically based on the warping deformation model. The dynamics of drilling tool predicted using rigid receptance coupling model are seen to agree well with the experimental results. All the natural frequencies are predicted with less than 5% error. The difference of the natural frequencies between the flexible receptance coupling model and the experimental results are less than 12%. The higher percentage errors using flexible receptance coupling compared to rigid receptance coupling are probably due to complex non-linear damping at the joint and the measurement error in hammer tests. In rigid receptance coupling model, as the joint is an integrated part of substructure B, the damping parameters of the joint are included in the measured dynamics of substructure B. Large discrepancy of the FRFs' peak amplitudes is observed in Figure 4.14 in comparing the predicted results by the proposed model and the experimental measurements. The reason is that the peak amplitude is sensitive to the alignment in the hammer test setup. Furthermore, the FRF amplitude is highly influenced by the damping of the structure, which has to be calibrated through experimental procedure. In this study, the damping coefficient is obtained from the drilling tool in free-free boundary condition, and then used in RC technique to obtain the FRF of tool-fixture assembly.

Chatter stability lobes predicted by the FRFs from the proposed model, the experimental measurements and the cantilever approximation are shown in Figure 4.18. Only torsional-axial vibration of the drilling tool is considered, and CutPro is used to simulate the results. Spindle speed in the range of 5 k to 20 k RPM is investigated because of small tool diameter. The low radial depth of cut is due to the small diameter and long aspect ratio of the drilling tool. It is shown that the proposed model considering the dynamics of clamping boundary is able to improve the prediction accuracy compared to cantilever boundary assumption. However, the error of critical radial depth of cut predicted by the proposed model is 20% compared to the value obtained from experimental FRFs. It is due to the error in predicting the amplitude of the FRFs from the model. Furthermore, Figure 4.14 shows the non-symmetry between axial-torsional and torsional-axial FRFs of the drilling tool, which is caused by the non-linearity of the system and the measurement error in the hammer tests. When the hammer is applied to excite the torsional vibration of the drilling tool, it cannot perfectly hit along the tangential direction of the drilling tool's cross section. Any deviation in the direction causes error in the magnitude of the FRFs, therefore resulting in the non-symmetric FRF results. Chatter stability lobe assuming symmetric cross FRF based on the result in axial-torsional direction is simulated, and it is found that the results from symmetric and non-symmetric FRFs are the same. It is because the axial- torsional FRF has higher amplitude compared to torsional-axial FRF based on Figure 4.14, and it dominates the generation of stability lobe.

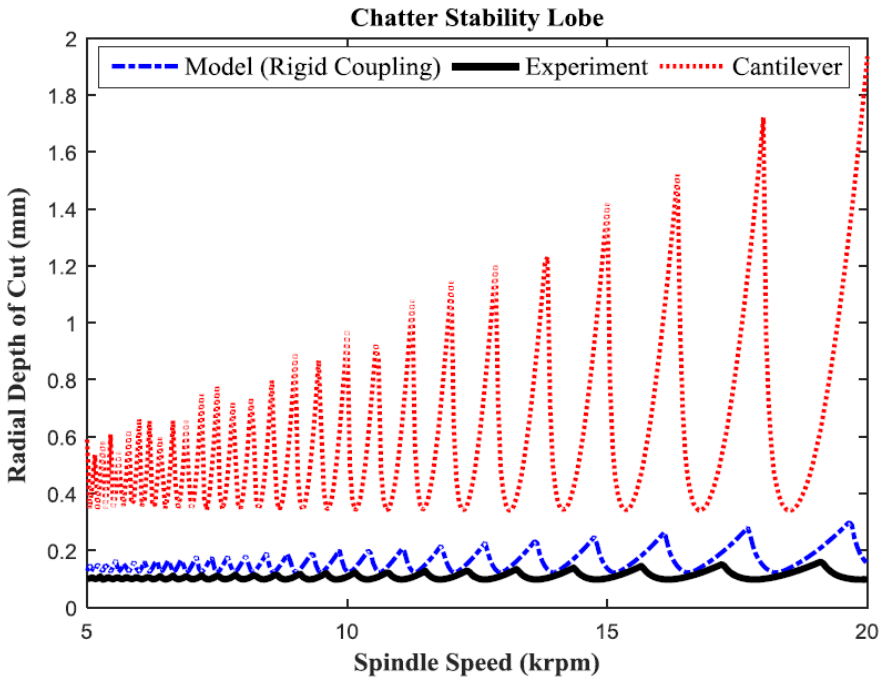

Figure 4.18 Chatter stability lobes due to torsional-axial vibration

The proposed rigid RC method finds its most common application in the case of micro drills whose dynamics are greatly influenced by clamping boundary conditions compared to conventional drilling tools. Most of the micro drills generally have the same shank diameter (1/8'') and the fluted portion is attached to the shank by taper and circular sections. If a blank tool with diameter the same as that of shank is modeled as substructure B and the dynamics of the chuck are measured, numerical modeling can be performed for the taper and flute section of the micro drill, and then coupled to the shank using rigid receptance coupling method. Therefore, dynamics of micro-drills can be predicted without repetitive measurements of FRFs. This proves to be an efficient method where a number of micro drilling tools are used, and prediction of dynamics experimentally is not possible for each tool. However, in the case of conventional drills, flexible receptance coupling technique is able to calibrate the joint dynamics near the tool holder, and the torsional-axial dynamics of a number of drilling tools with various geometric parameters can be predicted.

CHAPTER V

CONCLUSIONS AND RECOMMENDATIONS

5.1 Conclusions

This thesis presents a two-dimensional FE model to investigate the effects of warping on the coupled torsional-axial vibration behavior of a drilling tool. Natural frequencies and mode shapes corresponding to coupled torsional-axial vibration are predicted and experimentally validated with impact tests on the drilling tool using Laser Doppler Vibrometer. The effect of critical geometric parameters that directly influence the warping cross section properties of the drilling tool on the coupled torsional-axial dynamics is analyzed. This analysis based on the proposed model provides an efficient way to provide optimum geometric configuration for required dynamic behavior. The following conclusions are drawn based on this study:

(1) Solution to warping function of the drilling tool cross section is obtained through Prandtl's stress function approach and different cross section properties that are dependent on warping deformation of drilling tool cross section are determined. A two-dimensional FE model is used to derive the cross section constants that influence the coupled torsional-axial dynamics of the drilling tool.

(2) Natural frequencies and Mode shapes of a conventional drilling tool corresponding to the coupled torsional-axial vibration of the drilling tool are predicted. The predicted results are experimentally validated by impact testing on the drilling tool using Laser Doppler Vibrometer and also using a commercial FE software. It is observed that the proposed model was able to predict the natural frequencies of the conventional drilling tool with less than 6% error when compared with commercial FE and experimental results. The mode shapes predicted from the model are validated by the experimental results.

(3) The effects of Helix angle, Web thickness and Aspect ratio on the coupled torsional-axial dynamic behavior of a conventional drilling tool are predicted for the first three natural frequencies. It is observed that the change in helix angle and web thickness of the tool is more for torsion dominant modes and very little changes are observed in axial dominant modes. This is because warping deformation of the cross section does not have any influence on the axial modes of the drilling tool. But with increase in aspect ratio, all the three natural frequencies are seen to decrease because of the fact that the vibration in both axial and torsion dominant modes is inversely proportional to the length of the beam.

(4) The proposed model is applied to determine the natural frequencies of a micro drilling tool also. The predicted results are having less than 3% error when compared with a commercial FE software.

(5) The effects of helix angle and web thickness of the micro drilling tool on its coupled torsional-axial dynamics are analyzed. It is found that the natural frequencies corresponding to the torsion vibration dominance of fluted portion of the micro drill changes, but the shank dominant modes and axial vibration dominant flute modes are not affected. With increase in aspect ratio, all the natural frequencies are seen to decrease.

An enhanced receptance coupling model considering the coupling between torsional and axial vibrations of the drilling tool is developed and applied to study the effects of clamping boundary conditions on the coupled torsional-axial dynamics of drilling tool. Rigid and flexible receptance coupling are applied, and the dynamic results of the assembled structures are predicted with experimental validation. The following conclusions are drawn based on this study:

(1) Coupled torsional-axial dynamics of the tool tip are predicted using rigid receptance coupling model. Predicted FRFs are validated through impact test experiments. The first natural frequency is observed near 5.6 KHz which comes from the tool. Other peaks in the FRFs are influenced by the vibration of chuck and fixture and are different in in different types of vibration. It is also shown that cantilever approximation of drilling tool fixed in the holder fails to represent the accurate dynamics of the drilling process.

(2) Flexible receptance coupling technique is applied to predict the actual coupled torsional-axial dynamics of the drilling tool considering the clamping boundary condition. Tool point frequency response function is predicted using substructure analysis and validated with experimentally obtained FRF. Hence, the proposed receptance coupling technique can be reliable in predicting the actual dynamics of the drilling tool.

5.2 Recommendations for future work

Vibration assisted machining has been interesting research topic with many applications in the material removal processes for brittle materials. Through vibration assistance, thrust force can be reduced greatly leading to better hole quality. Study of the effect of vibration assistance on the negative effects of coupled torsional-axial vibrations are be suggested as future work.

Because of the small size and complex fluted geometry, impact testing on micro drills is a difficult task. Also, micro drills have a high range of natural frequencies typically more than 35 KHz whereas the miniature hammer has a highest bandwidth of less than 20 KHz. Due to this

limitation, experimental investigation of coupled torsional-axial dynamics is not included in this thesis. This can be a potential topic for the improvement of this work.

The proposed model can be applied to predict the chatter stability lobes corresponding to the coupled torsional-axial vibration behavior of the drilling tool. Prediction of chatter free cutting conditions from the proposed model would be an interesting extension to this work.

REFERENCES

[1] Altintas, Y.,2012, Manufacturing Automation, Cambridge University, Cambridge, UK.

[2] Roukema, J. C., & Altintas, Y. (2007). Generalized modeling of drilling vibrations. Part I:Time domain model of drilling kinematics, dynamics and hole formation. International Journal of Machine Tools and Manufacture, 47(9), 1455-1473.

[3] dreamstime. Drilling into a block of metal with a lot of cuttings. Retrieved from http://www.dreamstime.com/royalty-free-stock-photos-drilling-block-metal-image20020938

[4] CNC micro drilling. Retrieved from http://www.datron.com/applications/micro-drilling.php

[5] RIFF company, Inc. Micro Drilling and Machining. Retrieved from http://www.riff-co.com/machine.htm

[6] SECO tools, Monoblock micro drill bit. Retrieved from http://www.directindustry.com/prod/seco-tools/product-5699-763823.html

[7] POTOMAC. Small hole drilling. Retrieved from http://www.potomac-laser.com/services/core/micro-hole-drilling/

[8] Evolution Performance. Aerospace Components Drag Brake Kit 2007-2009 Shelby GT 500. Retrieved from http://www.evoperform.com/shop/index.php?manufacturers_id=39

[9] Bayly, P. V., Metzler, S. A., Schaut, A. J., & Young, K. A. (2001). Theory of torsional chatter in twist drills: model, stability analysis and composition to test. Journal of Manufacturing Science and Engineering, 123(4), 552-561.

[10] Wagner, H., & Pretschner, W. (1936). Torsion and buckling of open sections. National Advisory Committee for Aeronautics.

[11] Schmitz, T. L., & Smith, K. S. (2011). Mechanical vibrations: modeling and measurement. Springer Science & Business Media.

[12] Biot, M. A. (1939). Increase of torsional stiffness of a prismatical bar due to axial tension. Journal of Applied Physics, 10(12), 860-864

[13] Chu, C. (1951). The effect of initial twist on the torsional rigidity of thin prismatical bars and tubular members. Journal of Applied Mechanics-transactions of the ASME, 18(3), 337-337.

[14] Rosen, A. (1980). The effect of initial twist on the torsional rigidity of beams—another point of view. Journal of Applied Mechanics, 47(2), 389-392.

[15] Rosen, A. (1983). Theoretical and experimental investigation of the nonlinear torsion and extension of initially twisted bars. Journal of Applied Mechanics, 50(2), 321-326.

[16] Hodges, D. H. (1980). Torsion of pretwisted beams due to axial loading. Journal of Applied Mechanics, 47(2), 389-392.
[17] de Saint-Venant, M. (1856). Mémoire sur la torsion des prismes: avec des considérations sur leur flexion ainsi que sur l'équilibre intérieur des solides élastiques en général: et des formules pratiques pour le calcul de leur résistance à divers efforts s' exerçant simultanément. Imprimerie nationale.
[18] Shield, R. T. (1982). Extension and torsion of elastic bars with initial twist. Journal of Applied Mechanics, 49(4), 779-786.
[19] Krenk, S. (1983). A linear theory for pretwisted elastic beams. Journal of Applied Mechanics, 50(1), 137-142.
[20] Krenk, S. (1983). The torsion-extension coupling in pretwisted elastic beams. International Journal of Solids and Structures, 19(1), 67-72.
[21] Kosmatka, J. B. (1992). On the behavior of pretwisted beams with irregular cross-sections. Journal of Applied Mechanics, 59(1), 146-152.
[22] Rosen, A. (1991). Structural and dynamic behavior of pretwisted rods and beams. Applied Mechanics Reviews, 44(12), 483-515.
[23] Liu, K. C., Friend, J., & Yeo, L. (2009). The axial–torsional vibration of pretwisted beams. Journal of Sound and Vibration, 321(1), 115-136.
[24] Theocaris, P. S. (1989). The warping functions of regular prismatic bars under torsion evaluated by caustics. Experimental Mechanics, 29(3), 285-290.
[25] Krahula, J. L., & Lauterbach, G. F. (1969). A finite element solution for Saint-Venant torsion. AIAA Journal, 7(12), 2200-2203.
[26] Prandtl, L. (1903). 'Zur torsion yon prismatischen Staeben,'. Physik. Zeitsch., 4, 758, 770.
[27] Alberty, J., Carstensen, C., & Funken, S. A. (1999). Remarks around 50 lines of Matlab: short finite element implementation. Numerical Algorithms, 20(2-3), 117-137.
[28] Mixon, B. D. (2008). The Development Of A Finite Element Tool For The Calculation Of Beam Cross Section Properties. ProQuest.
[29] Roukema, J. C., & Altintas, Y. (2006). Time domain simulation of torsional–axial vibrations in drilling. International Journal of Machine Tools and Manufacture, 46(15), 2073-2085.
[30] Roukema, J. C., & Altintas, Y. (2007). Generalized modeling of drilling vibrations. Part II: Chatter stability in frequency domain. International Journal of Machine Tools and Manufacture, 47(9), 1474-1485.
[31] Moetakef Imani, B., & Moosavi, S. G. (2009, October). Time domain simulation of torsional-axial and lateral vibration in drilling operation. In International Conference on Applications and Design in Mechanical Engineering-ICADME.
[32] Ahmadi, K., & Altintas, Y. (2013). Stability of lateral, torsional and axial vibrations in drilling. International Journal of Machine Tools and Manufacture,68, 63-74.

[33] Voronov, S. A., Gouskov, A. M., Kvashnin, A. S., Butcher, E. A., & Sinha, S. C. (2007). Influence of torsional motion on the axial vibrations of a drilling tool. Journal of computational and nonlinear dynamics, 2(1), 58-64.
[34] Filiz, S., & Ozdoganlar, O. B. (2009). Coupled torsional-axial vibrations of micro- and macro-drills. Trans. NAMRI/SME, 37, 57-65.
[35] Yagci, B., Filiz, S., Romero, L. L., & Ozdoganlar, O. B. (2009). A spectral-Tchebychev technique for solving linear and nonlinear beam equations. Journal of Sound and Vibration, 321(1), 375-404.
[36] Filiz, S., & Ozdoganlar, O. B. (2011). A three-dimensional model for the dynamics of micro-endmills including bending, torsional and axial vibrations. Precision Engineering, 35(1), 24-37.
[37] Filiz, S., Ozdoganlar, O. B., & Romero, L. A. (2008). An analytical model for micro-endmill dynamics. Journal of Vibration and Control.
[38] Filiz, S., & Ozdoganlar, O. B. (2010). A Model for Bending, Torsional, and Axial Vibrations of Micro-and Macro-Drills Including Actual Drill Geometry—Part I: Model Development and Numerical Solution. Journal of Manufacturing Science and Engineering, 132(4), 041017.
[39] Filiz, S., & Ozdoganlar, O. B. (2010). A Model for Bending, Torsional, and Axial Vibrations of Micro-and Macro-Drills Including Actual Drill Geometry—Part II: Model Validation and Application. Journal of Manufacturing Science and Engineering, 132(4), 041018.
[40] Filiz, S., & Ozdoganlar, O. B. (2008). Experimental modal analysis of micro-drills. Trans. NAMRI/SME, 36, 185-192.
[41] Schmitz, T. L., & Donalson, R. R. (2000). Predicting high-speed machining dynamics by substructure analysis. CIRP Annals-Manufacturing Technology,49(1), 303-308.
[42] Schmitz, T. L., Davies, M. A., & Kennedy, M. D. (2001). Tool point frequency response prediction for high-speed machining by RCSA. Journal of Manufacturing Science and Engineering, 123(4), 700-707.
[43] Park, S. S., Altintas, Y., & Movahhedy, M. (2003). Receptance coupling for end mills. International Journal of Machine Tools and Manufacture, 43(9), 889-896.
[44] Mascardelli, B. A., Park, S. S., & Freiheit, T. (2006). Substructure Coupling of Micro-End Mills. In ASME 2006 International Mechanical Engineering Congress and Exposition (pp. 145-150).
[45] Schmitz, T. L., & Duncan, G. S. (2006). Receptance coupling for dynamics prediction of assemblies with coincident neutral axes. Journal of Sound and Vibration, 289(4), 1045-1065.
[46] Schmitz, T. L., & Duncan, G. S. (2005). Three-component receptance coupling substructure analysis for tool point dynamics prediction. Journal of Manufacturing Science and Engineering, 127(4), 781-790.
[47] Park, S. S., & Chae, J. (2008). Joint identification of modular tools using a novel receptance coupling method. The International Journal of Advanced Manufacturing Technology, 35(11-12), 1251-1262.
[48] Chae, J., Park, S. S., & Lin, S. (2011). Substructure coupling with joint identification for reconfigurable manufacturing systems. Proceedings of the Canadian Engineering Education Association.

[49] Schmitz, T. L. (2010). Torsional and axial frequency response prediction by RCSA. Precision Engineering, 34(2), 345-356.
[50] Tsai, W. D., & Wu, S. M. (1979). Computer analysis of drill point geometry. International Journal of Machine Tool Design and Research, 19(2), 95-108.
[51] Fujii, S., DeVries, M. F., & Wu, S. M. (1970). An analysis of drill geometry for optimum drill design by computer. Part I—drill geometry analysis. Journal of Manufacturing Science and Engineering, 92(3), 647-656.
[52] Vijayaraghavan, A., & Dornfeld, D. A. (2007). Automated drill modeling for drilling process simulation. Journal of Computing and Information Science in Engineering, 7(3), 276-282.
[53] Ecsedi, I., & Baksa, A. (2010). Prandtl's formulation for the Saint–Venant's torsion of homogeneous piezoelectric beams. International Journal of Solids and Structures, 47(22), 3076-3083.
[54] Chandrupatla, T. R., Belegundu, A. D., Ramesh, T., & Ray, C. (1997).Introduction to finite elements in engineering (pp. 279-300). Upper Saddle River: Prentice Hall.
[55] CUTPRO™. (2001). Advanced Milling Process Simulation System. http://www.malinc.com.
[56] SolidWorks, I. (2002). Dassault Systèmes, Solidworks Corporation.
[57] Marlow F M, Tallman P J (2010) Machine Shop Know-How, Metal Arts Press, California.
[58] Cao, H., Xi, S., & Cheng, W. (2015). Model Updating of Spindle Systems Based on the Identification of Joint Dynamics. Shock and Vibration, 2015, 10. doi:10.1155/2015/89430

APPENDICES

APPENDIX 1

The derivation of the warping constants based on the proposed model is given below:

$$S = \iint_A \left(y^2 + z^2 + y\frac{\partial \Phi}{\partial \mathrm{y}} + z\frac{\partial \Phi}{\partial z}\right) dy\, dz$$

$$= \iint_A (y^2)\ \ dy\, dz + \iint_A (z^2)\ \ dy\, dz + \iint_A \left(y\frac{\partial \Phi}{\partial \mathrm{y}}\right)\ \ dy\, dz + \iint_A \left(z\frac{\partial \Phi}{\partial z}\right)\ \ dy\, dz \qquad (A1)$$

By substituting Equation (9) into the above equation, the elemental interpolation of the constant S in Equation (A1) can be expressed as:

$$S = \iint_A (N_1 y_1 + N_2 y_2 + N_3 y_3)^2\ \ dy\, dz + \iint_A (N_1 z_1 + N_2 z_2 + N_3 z_3)^2\ \ dy\, dz$$
$$+ \iint_A (N_1 y_1 + N_2 y_2 + N_3 y_3)\left(\frac{\partial (N_1\Phi_1 + N_2\Phi_2 + N_3\Phi_3)}{\partial \mathrm{y}}\right) dy\, dz$$
$$+ \iint_A (N_1 z_1 + N_2 z_2 + N_3 z_3)\left(\frac{\partial (N_1\Phi_1 + N_2\Phi_2 + N_3\Phi_3)}{\partial z}\right) dy\, dz$$

$$S = \iint_A (\, N_1^2 y_1^2 + 2N_1 N_2 y_1 y_2 + N_2^2 y_2^2 + 2N_1 N_3 y_1 y_3 + 2N_2 N_3 y_2 y_3 + N_3^2 y_3^2)\; dy\, dz$$

$$+ \iint_A (\, N_1^2 z_1^2 + 2N_1 N_2 z_1 z_2 + N_2^2 z_2^2 + 2N_1 N_3 z_1 z_3 + 2N_2 N_3 z_2 z_3 + N_3^2 z_3^2)\; dy\, dz$$

$$+ \iint_A (\Phi_1 N_1 y_1 \frac{\partial N_1}{\partial \mathrm{y}} + \Phi_2 N_1 y_1 \frac{\partial N_2}{\partial \mathrm{y}} + \Phi_3 N_1 y_1 \frac{\partial N_3}{\partial \mathrm{y}} + \Phi_1 N_2 y_2 \frac{\partial N_1}{\partial \mathrm{y}}$$

$$+ \Phi_2 N_2 y_2 \frac{\partial N_2}{\partial \mathrm{y}} + \Phi_3 N_2 y_2 \frac{\partial N_3}{\partial \mathrm{y}} + \Phi_1 N_3 y_3 \frac{\partial N_1}{\partial \mathrm{y}} + \Phi_2 N_3 y_3 \frac{\partial N_2}{\partial \mathrm{y}}$$

$$+ \Phi_3 N_3 y_3 \frac{\partial N_3}{\partial \mathrm{y}})\; dy\, dz$$

$$+ \iint_A (\Phi_1 N_1 z_1 \frac{\partial N_1}{\partial \mathrm{z}} + \Phi_2 N_1 z_1 \frac{\partial N_2}{\partial \mathrm{z}} + \Phi_3 N_1 z_1 \frac{\partial N_3}{\partial \mathrm{z}} + \Phi_1 N_2 z_2 \frac{\partial N_1}{\partial \mathrm{z}}$$

$$+ \Phi_2 N_2 z_2 \frac{\partial N_2}{\partial \mathrm{z}} + \Phi_3 N_2 z_2 \frac{\partial N_3}{\partial \mathrm{z}} + \Phi_1 N_3 z_3 \frac{\partial N_1}{\partial \mathrm{z}} + \Phi_2 N_3 z_3 \frac{\partial N_2}{\partial \mathrm{z}}$$

$$+ \Phi_3 N_3 z_3 \frac{\partial N_3}{\partial \mathrm{z}})\; dy\, dz \qquad (A2)$$

From Equation (8), we get $\frac{\partial N_1}{\partial \mathrm{y}} = \frac{b_1}{2A_e}, \frac{\partial N_2}{\partial \mathrm{y}} = \frac{b_2}{2A_e}, \frac{\partial N_3}{\partial \mathrm{y}} = \frac{b_3}{2A_e}, \frac{\partial N_1}{\partial \mathrm{z}} = \frac{c_1}{2A_e}, \frac{\partial N_2}{\partial \mathrm{z}} = \frac{c_2}{2A_e}, \frac{\partial N_3}{\partial \mathrm{z}} = \frac{c_3}{2A_e}$.

Substituting in Equation (A2),

$$S = \iint_A (\, N_1^2 y_1^2 + 2N_1N_2y_1y_2 + N_2^2 y_2^2 + 2N_1N_3y_1y_3 + 2N_2N_3y_2y_3 + N_3^2 y_3^2)\; dy\, dz$$

$$+ \iint_A (\, N_1^2 z_1^2 + 2N_1N_2z_1z_2 + N_2^2 z_2^2 + 2N_1N_3z_1z_3 + 2N_2N_3z_2z_3 + N_3^2 z_3^2)\; dy\, dz$$

$$+ \frac{1}{2A_e} \iint_A (\Phi_1 N_1 y_1\, b_1 + \Phi_2 N_1 y_1\, b_2 + \Phi_3 N_1 y_1\, b_3 + \Phi_1 N_2 y_2\, b_1 + \Phi_2 N_2 y_2\, b_2$$

$$+ \Phi_3 N_2 y_2\, b_3 + \Phi_1 N_3 y_3\, b_1 + \Phi_2 N_3 y_3\, b_2 + \Phi_3 N_3 y_3\, b_3)\;\; dy\, dz$$

$$+ \frac{1}{2A_e} \iint_A (\Phi_1 N_1 z_1\, c_1 + \Phi_2 N_1 z_1\, c_2 + \Phi_3 N_1 z_1\, c_3 + \Phi_1 N_2 z_2\, c_1 + \Phi_2 N_2 z_2\, c_2$$

$$+ \Phi_3 N_2 z_2\, c_3 + \Phi_1 N_3 z_3\, c_1 + \Phi_2 N_3 z_3\, c_2 + \Phi_3 N_3 z_3\, c_3)\;\; dy\, dz \qquad (A3)$$

By using Equation (10) in Equation (A3), it is obtained that:

$$S = \frac{A_e}{6}[y_1^2 + y_2^2 + y_3^2 + y_1y_2 + y_2y_3 + y_1y_3] + \frac{A_e}{6}[z_1^2 + z_2^2 + z_3^2 + z_1z_2 + z_2z_3 + z_1z_3]$$

$$+ \frac{1}{6}[b_1y_1\Phi_1 + b_2y_1\Phi_2 + b_1y_1\Phi_3 + b_1y_2\Phi_1 + b_2y_2\Phi_2 + b_3y_2\Phi_3 + b_1y_3\Phi_1$$

$$+ b_2y_3\Phi_2 + b_3y_3\Phi_3]$$

$$+ \frac{1}{6}[c_1z_1\Phi_1 + c_2z_1\Phi_2 + c_1z_1\Phi_3 + c_1z_2\Phi_1 + c_2z_2\Phi_2 + c_3z_2\Phi_3 + c_1z_3\Phi_1$$

$$+ c_2z_3\Phi_2 + c_3z_3\Phi_3] \qquad (A4)$$

The warping constants *K*, *D* and *F* in Equation (12) can be evaluated in their elemental forms using the shape functions in the same manner.

VITA

Narahara Gopal Koya

Candidate for the Degree of

Master of Science

Thesis: INVESTIGATION OF WARPING EFFECT ON COUPLED TORSIONAL-AXIAL VIBRATIONS OF DRILLING TOOL

Major Field: Mechanical and Aerospace Engineering

Biographical:

Education:

Completed the requirements for the Master of Science degree in Mechanical and Aerospace Engineering at Oklahoma State University, Stillwater, Oklahoma in December, 2015.

Received Bachelor of Technology degree in Mechanical Engineering from Acharya Nagarjuna University, Guntur, Andhra Pradesh in 2013.

Experience:

- Graduate Research Assistant in Precision Manufacturing Processes Laboratory (PMPL) at Oklahoma State University, Stillwater, Oklahoma.

- Graduate Teaching Assistant for Engineering Design CAD at Oklahoma State University, Stillwater, Oklahoma.